High order conservative Lagrangian scheme for three-temperature radiation hydrodynamics

Juan Cheng¹, Nuo Lei ², and Chi-Wang Shu³

Abstract

The three-temperature (3-T) radiation hydrodynamics (RH) equations are widely used in modeling various optically thick high-energy-density-physics environments, such as those in astrophysics and inertial confinement fusion (ICF). In this paper, we will discuss the methodology to construct a high order conservative Lagrangian scheme solving 3-T RH equations. Specifically, the three new energy variables are defined first, in the form of which the three energy equations of the 3-T RH equations are rewritten. The main advantage of this formulation is that it facilitates the design of a scheme with both conservative property and arbitrary high order accuracy. Starting from one dimension and based on the multi-resolution WENO reconstruction and the strong stability preserving (SSP) high order time discretizations, taken as an example, we design a third order conservative Lagrangian scheme both in space and time. To determine the numerical flux for the conservative advection terms in the 3-T RH equations, we propose a HLLC numerical flux which is derived from the divergence theorem rigorously and is suitable for multi-material problems with the ideal-gas equations of state. After that, we discuss how to design a class of high order positivity-preserving explicit Lagrangian schemes to solve the 3-T RH equations which only contain the conservative advection terms in space. Preliminary extension to the two dimensional case is also considered. Finally, various numerical tests are given to verify the desired properties of the high order Lagrangian schemes such as high order accuracy, non-oscillation, conservation and adaptation to multi-material problems.

Keywords: Lagrangian method; high order; HLLC flux; radiation hydrodynamics equations; three-temperature

AMS subject classification: 65M08

¹Corresponding author. Laboratory of Computational Physics, Institute of Applied Physics and Computational Mathematics, Beijing 100088, China and HEDPS, Center for Applied Physics and Technology, and College of Engineering, Peking University, Beijing 100871, China. E-mail: cheng_juan@iapcm.ac.cn. Research is supported in part by National Key R&D Program of China No. 2022YFA1004500, and NSFC grant 12031001.

²LSEC, Institute of Computational Mathematics, Hua Loo-Keng Center for Mathematical Sciences, Academy of Mathematics and Systems Science, Chinese Academy of Sciences, Beijing 100190, P.R. China. E-mail: nuo_lei@lsec.cc.ac.cn. Research is part by supported by NSFC grant 12288201.

³Division of Applied Mathematics, Brown University, Providence, RI 02912, USA. E-mail: chi-wang_shu@brown.edu. Research is supported in part by NSF grants DMS-2010107 and DMS-2309249.

1 Introduction

In astrophysics and inertial confinement fusion (ICF) and some other high-energy-density-physics fields, there is the phenomenon of the interaction between radiation and plasmas, called radiation hydrodynamics (RH). High-energy-density plasmas contain electrons and ions. The electrons and ions usually have different temperatures since the ions are preheated by shock waves, the electrons are preheated or cooled through the interaction with the radiation field etc. In the optically thick limit, radiation can also be described by its own temperature. Thus, in this case, there are three temperatures to describe the electron, ion and radiation respectively. The evolution of the interaction between radiation and plasmas can be governed by the three-temperature (3-T) radiation hydrodynamics (RH) equations. The 3-T RH equations are widely used in modeling various optically thick high-energy-density-physics environments [3, 13, 22].

The 3-T RH equations consist of the advection, diffusion and energy-exchange terms which are highly nonlinear and tightly coupled. The terms also possess multiple scales. Moreover, in the fields such as astrophysics and ICF, the RH equations usually describe the interaction between radiation and multi-material matter, where accurate calculation of the material interfaces is critical. The 3-T RH equations are widely adopted in many astrophysics and ICF codes such as CRASH, FLASH and RAGE [19, 16, 17].

The 3-T RH system is of a nonconservative form (see (2.1)), which brings much difficulty to the design of a good numerical method to solve it. In fact, solving the nonconservative hyperbolic system is a delicate job due to the definition of weak admissible solutions. It has been demonstrated by Abgrall and Karni [1] that those numerical schemes designed to solve the nonconservative hyperbolic equations directly may fail to converge to the right solutions. Only when the partial differential equations (PDEs) are written in the conservative form, can we easily design a scheme which could keep the conservation. By the Lax-Wendroff theorem, we know that the conservative property is a very critical issue for the numerical method solving the advection-dominated PDEs such as the 3-T RH equations, since only the result of a conservative numerical method can be trusted to converge to the weak solution of the PDEs, which could guarantee the correct speed of discontinuities such as shocks and contacts.

There are some pioneering works on designing conservative schemes solving the RH equations in the nonconservative form in the literature. In [28], by solving the equations of total energy and electron energy directly, the authors proposed a conservative numerical scheme for the two-temperature nonequilibrium model so that it could avoid the solution with non-physical shocks. In [4], the authors presented an arbitrary Lagrangian Eulerian (ALE)

method to simulate multi-material fluid flows on a two-temperature (ion and electron) hydrodynamics model. In order to preserve the conservation, the total energy equation is solved at the Lagrangian step. In [9], by the establishment of an equivalency relationship between the discretizations of the equations in the forms of the total energy and of the internal energy, the cell-centered conservative Lagrangian schemes were designed to solve one and multiple nonconservative internal energy equations directly. In [25, 6], the authors followed the idea proposed by Abgrall in [2] and employed a structure-preserving strategy on the two-temperature and three-temperature RH models respectively, which is based on the key concept that mathematical structures associated with conservative and nonconservative equations are preserved, even at the discrete level. The proposed schemes maintain global conservation errors within the round-off level. Although the above mentioned schemes can keep the conservation, their accuracy is at most second order, and it is very difficult to generalize them to higher order accuracy (especially higher order in time). Even though ample progress has been made, the design of conservative schemes for shock solutions to nonconservative systems and their numerical analysis are far from complete.

The investigation of numerical methods on the three-temperature nonequilibrium models has become an active research topic in recent years. There are several literatures focusing on the discretization of the 3-T diffusion equations, for example, in [14], the authors built a convex combination-based scheme which unconditionally satisfies a maximum principle, at each sub-iteration of the non-linear iterative process. For the more complicated fully 3-T RH equations (2.1), there are much less discussion on their numerical methods. In [26, 27], a 3-T, unstructured-grid, non-equilibrium RH code was developed for the simulation of intense thermal radiation or high-power laser driven radiative shock hydrodynamics in two-dimensional (2D) axis-symmetric geometries based on the Lagrangian method. In [6], a first order positivity-preserving, conservative and entropy-stable numerical scheme was presented for the 3-T RH model. In [15], the numerical comparisons between three simulation codes solving 3-T RH models were given. In summary, all the above mentioned methods for the 3-T radiative diffusion and radiation hydrodynamics models are at most second order accurate in space and time.

In this paper, we will discuss the methodology to construct a high order conservative Lagrangian scheme solving one dimensional 3-T RH equations (2.1). We will also briefly discuss the extension to two dimensions. To be specific, we first define three new energy variables and rewrite the three energy equations in the 3-T RH equations (2.1) in the form of these variables. In the new form of the 3-T RH equations, we can easily design a conservative Lagrangian scheme. Besides the maintenance of the conservative property, the major advantage of this approach is that the scheme can be easily designed to arbitrary high order

accuracy both in space and time. In this paper, based on the multi-resolution WENO reconstruction [30] and the strong stability preserving (SSP) or total variation diminishing (TVD) high order time discretizations [23, 18], taking as an example, we design a third order conservative Lagrangian schemes both in space and time. To solve the conservative advection terms of 3-T RH equations, we further propose a HLLC numerical flux which is derived from the divergence theorem rigorously and is applicable for the multi-material problems with the ideal-gas equations of state. After that, we discuss how to design a class of high order positivity-preserving explicit Lagrangian schemes to solve the 3-T RH equations which only contain the conservative advection terms in space. Then, we extend our one-dimensional high order Lagrangian scheme to the two-dimensional case. Finally various numerical tests are given to verify the desired properties of the high order Lagrangian schemes such as high order accuracy, non-oscillation, conservation and adaptation to multi-material problems.

An outline of the rest of this paper is as follows. In Section 2, we rewrite the system to facilitate the design of conservative schemes, and document the Jacobian and its eigen values and eigen vectors to establish hyperbolicity of the convection terms and to help in local characteristic decompositions needed for high order schemes. In Section 3, we describe a third order explicit Lagrangian scheme solving the 1D 3-T RH equations. In Section 4, we discuss the issue of positivity-preserving for the high order Lagrangian scheme. In Section 5, we briefly discuss the two-dimensional high order Lagrangian scheme for the 2D 3-T RH equations. In Section 6, several numerical examples are given to verify the performance of the new Lagrangian schemes. In Section 7 we will give concluding remarks.

2 One dimensional three temperature radiation hydrodynamics equations

We consider the three-temperature radiation hydrodynamics equations, which has the following form in one dimensional Cartesian coordinate,

$$\begin{cases}
\partial_{t}\rho + \partial_{x}\rho u = 0 \\
\partial_{t}\rho u + \partial_{x}(\rho u^{2} + p_{e} + p_{i} + p_{r}) = 0 \\
\partial_{t}\rho e_{e} + \partial_{x}\rho e_{e}u + p_{e}\partial_{x}u = \partial_{x}(\kappa_{e}\partial_{x}T_{e}) - \omega_{ei}(T_{e} - T_{i}) - \omega_{er}(T_{e}^{4} - T_{r}^{4}) \\
\partial_{t}\rho e_{i} + \partial_{x}\rho e_{i}u + p_{i}\partial_{x}u = \partial_{x}(\kappa_{i}\partial_{x}T_{i}) + \omega_{ei}(T_{e} - T_{i}) \\
\partial_{t}\rho e_{r} + \partial_{x}\rho e_{r}u + p_{r}\partial_{x}u = \partial_{x}(\kappa_{r}\partial_{x}T_{r}^{4}) + \omega_{er}(T_{e}^{4} - T_{r}^{4})
\end{cases} (2.1)$$

Here, ρ is the density, u is the velocity. $\{e_e, e_i, e_r\}$, $\{p_e, p_i, p_r\}$ and $\{T_e, T_i, T_r\}$ are the specific internal energy, pressure and temperature for electron, ion and radiation respectively. $\{\kappa_e, \kappa_i, \kappa_r\}$ are the conduction coefficients of electron, ion, and radiation respectively. ω_{ei}, ω_{er} are the energy-exchange coefficients between electron and ion, and between electron and

radiation respectively. The system (2.1) represents the conservation of mass, momentum and total energy, where the total energy is defined as $E = \rho(e_e + e_i + e_r) + \frac{1}{2}\rho u^2$. The three specific internal energies are related to the corresponding temperatures as $e_r = aT_r^4/\rho$, $e_e = c_{ve}T_e$ and $e_i = c_{vi}T_i$, where a is the radiation constant, c_{ve} and c_{vi} are the heat capacity at constant volume of electron and ion respectively.

The set of equations needs to be completed by the addition of the matter's equations of state (EOS) with the following general form,

$$p_e = p(\rho, e_e), \qquad p_i = p(\rho, e_i). \tag{2.2}$$

Especially, if we consider the γ -law gas, then the equations of state (EOS) have the following simpler form,

$$p_e = (\gamma_e - 1)\rho e_e, \qquad p_i = (\gamma_i - 1)\rho e_i, \tag{2.3}$$

where γ_e, γ_i are the constants representing the ratio of specific heat capacities of the electron and ion respectively. The "EOS" for radiation is given simply as $p_r = \frac{1}{3}\rho e_r$. In order to present the formulation of the eigenvalues and eigenvectors for the advection terms of (2.1) in a more symmetric way, we rewrite p_r in the similar form as p_e, p_i , that is,

$$p_r = (\gamma_r - 1)\rho e_r \tag{2.4}$$

where $\gamma_r = \frac{4}{3}$.

Notice that the last three energy equations in the system (2.1) are written in the nonconservative form, which brings much difficulty to the design of a conservative numerical method. To facilitate the design of high order Lagrangian schemes which could keep the conservation of mass, momentum and total energy, we introduce the following new "energy" variables,

$$E_e = \rho e_e + \frac{1}{6}\rho u^2, \quad E_i = \rho e_i + \frac{1}{6}\rho u^2, \quad E_r = \rho e_r + \frac{1}{6}\rho u^2,$$
 (2.5)

and then the system (2.1) can be rewritten as follows,

$$\begin{cases}
\partial_{t}\rho + \partial_{x}\rho u = 0 \\
\partial_{t}\rho u + \partial_{x}(\rho u^{2} + p_{e} + p_{i} + p_{r}) = 0 \\
\partial_{t}E_{e} + \partial_{x}((E_{e} + p_{e})u) - \frac{1}{3}u\partial_{x}(2p_{e} - p_{i} - p_{r}) = \partial_{x}(\kappa_{e}\partial_{x}T_{e}) - \omega_{ei}(T_{e} - T_{i}) - \omega_{er}(T_{e}^{4} - T_{r}^{4}) \\
\partial_{t}E_{i} + \partial_{x}((E_{i} + p_{i})u) - \frac{1}{3}u\partial_{x}(2p_{i} - p_{e} - p_{r}) = \partial_{x}(\kappa_{i}\partial_{x}T_{i}) + \omega_{ei}(T_{e} - T_{i}) \\
\partial_{t}E_{r} + \partial_{x}((E_{r} + p_{r})u) - \frac{1}{3}u\partial_{x}(2p_{r} - p_{e} - p_{i}) = \partial_{x}(\kappa_{r}\partial_{x}T_{r}^{4}) + \omega_{er}(T_{e}^{4} - T_{r}^{4}).
\end{cases} \tag{2.6}$$

We observe that the total energy is given by $E = E_e + E_i + E_r = \rho e_e + \rho e_i + \rho e_r + \frac{1}{2}\rho u^2$, and the left-hand sides of the last three equations in (2.6) are in conservation form except for the pressure differential convection terms.

We first consider the left hand side terms of the system (2.6) and rewrite them in the following form,

$$\frac{\partial \mathbf{U}}{\partial t} + A \frac{\partial \mathbf{U}}{\partial x} = 0 \tag{2.7}$$

where $\mathbf{U} = (\rho, \rho u, E_e, E_i, E_r)^T$.

If the ideal EOS (2.3) is considered, then the Jacobian matrix A related to the advection terms is as follows,

$$A = \begin{pmatrix} 0 & 1 & 0 & 0 & 0\\ \frac{(\gamma_e + \gamma_i + \gamma_r - 9)u^2}{6} & -\frac{(\gamma_e + \gamma_i + \gamma_r - 9)u}{3} & \gamma_e - 1 & \gamma_i - 1 & \gamma_r - 1\\ -\gamma_e e_e u + \frac{(\gamma_e + \gamma_i + \gamma_r - 6)}{18} u^3 & \gamma_e e_e - \frac{(2(\gamma_e + \gamma_i + \gamma_r) - 9)}{18} u^2 & \frac{(\gamma_e + 2)}{3} u & \frac{(\gamma_i - 1)}{3} u & \frac{(\gamma_r - 1)}{3} u\\ -\gamma_i e_i u + \frac{(\gamma_e + \gamma_i + \gamma_r - 6)}{18} u^3 & \gamma_i e_i - \frac{(2(\gamma_e + \gamma_i + \gamma_r) - 9)}{18} u^2 & \frac{(\gamma_e - 1)}{3} u & \frac{(\gamma_i + 2)}{3} u & \frac{(\gamma_r - 1)}{3} u\\ -\gamma_r e_r u + \frac{(\gamma_e + \gamma_i + \gamma_r - 6)}{18} u^3 & \gamma_r e_r - \frac{(2(\gamma_e + \gamma_i + \gamma_r) - 9)}{18} u^2 & \frac{(\gamma_e - 1)}{3} u & \frac{(\gamma_i - 1)}{3} u & \frac{(\gamma_r + 2)}{3} u \end{pmatrix}.$$

$$(2.8)$$

The matrix A has five eigenvalues as

$$\{u - c_s, u, u, u, u + c_s\}$$
(2.9)

where c_s is the sound speed given by

$$c_s = \sqrt{\gamma_e(\gamma_e - 1)e_e + \gamma_i(\gamma_i - 1)e_i + \gamma_r(\gamma_r - 1)e_r}.$$
(2.10)

We can see that all the above eigenvalues are real, which means the left hand side of the system (2.1) is hyperbolic. Denote

$$g_t = \gamma_e + \gamma_i + \gamma_r - 3, \quad g_e = \gamma_e - 1, \quad g_i = \gamma_i - 1, \quad g_r = \gamma_r - 1,$$

then the right eigenvectors of the matrix A are given as

$$\mathbf{R}_{1}(\mathbf{U}) = \begin{pmatrix} 1 \\ u - c_{s} \\ \gamma_{e}e_{e} + \frac{1}{6}u^{2} - \frac{1}{3}uc_{s} \\ \gamma_{i}e_{i} + \frac{1}{6}u^{2} - \frac{1}{3}uc_{s} \\ \gamma_{r}e_{r} + \frac{1}{6}u^{2} - \frac{1}{3}uc_{s} \end{pmatrix}, \mathbf{R}_{2}(\mathbf{U}) = \begin{pmatrix} 1 \\ u \\ \frac{1}{6}\frac{g_{t}}{g_{e}}u^{2} \\ g_{r} \\ -g_{i} \end{pmatrix}, \mathbf{R}_{3}(\mathbf{U}) = \begin{pmatrix} 1 \\ u \\ -g_{r} \\ \frac{1}{6}\frac{g_{t}}{g_{i}}u^{2} \\ g_{e} \end{pmatrix},$$

$$\mathbf{R}_{4}(\mathbf{U}) = \begin{pmatrix} 1 \\ u \\ g_{i} \\ -g_{e} \\ \frac{1}{6} \frac{g_{t}}{g_{r}} u^{2} \end{pmatrix}, \mathbf{R}_{5}(\mathbf{U}) = \begin{pmatrix} 1 \\ u + c_{s} \\ \gamma_{e} e_{e} + \frac{1}{6} u^{2} + \frac{1}{3} u c_{s} \\ \gamma_{i} e_{i} + \frac{1}{6} u^{2} + \frac{1}{3} u c_{s} \\ \gamma_{r} e_{r} + \frac{1}{6} u^{2} + \frac{1}{3} u c_{s} \end{pmatrix}.$$

Denote

$$H_{e} = 6g_{i}g_{r}(\gamma_{i}e_{i} - \gamma_{r}e_{r}) + \gamma_{e}g_{t}e_{e}u^{2},$$

$$H_{i} = 6g_{e}g_{r}(\gamma_{r}e_{r} - \gamma_{e}e_{e}) + \gamma_{i}g_{t}e_{i}u^{2},$$

$$H_{r} = 6g_{e}g_{i}(\gamma_{e}e_{e} - \gamma_{i}e_{i}) + \gamma_{r}g_{t}e_{r}u^{2},$$

$$b = g_{t}(36g_{e}g_{i}g_{r} + g_{t}u^{4})c_{s}^{2},$$
(2.11)

then the left eigenvectors of the matrix A can be written in the following form,

$$\mathbf{L}_{1}(\mathbf{U}) = \frac{1}{12c_{s}^{2}} \begin{pmatrix} u(g_{t}u + 6c_{s}) \\ -2(g_{t}u + 3c_{s}) \\ 6g_{e} \\ 6g_{r} \end{pmatrix}, \quad \mathbf{L}_{2}(\mathbf{U}) = \begin{pmatrix} \frac{g_{e}}{g_{t}} - \frac{g_{e}u^{2}}{6c_{s}^{2}} - \frac{g_{e}g_{t}u^{2}}{b}(H_{e} - u^{2}c_{s}^{2}) \\ \frac{g_{e}u}{3c_{s}^{2}} + \frac{2g_{e}g_{t}u}{b}(H_{e} - u^{2}c_{s}^{2}) \\ -\frac{g_{e}}{g_{t}c_{s}^{2}} - \frac{6g_{e}}{b}(g_{e}H_{e} - g_{t}u^{2}c_{s}^{2}) \\ -\frac{g_{e}g_{t}c_{s}^{2}}{g_{t}c_{s}^{2}} - \frac{6g_{e}g_{t}}{b}(H_{e} - 6g_{r}c_{s}^{2}) \\ -\frac{g_{e}g_{r}c_{s}^{2}}{g_{t}c_{s}^{2}} - \frac{6g_{e}g_{t}}{b}(H_{e} + 6g_{t}c_{s}^{2}) \end{pmatrix},$$

$$\mathbf{L}_{3}(\mathbf{U}) = \begin{pmatrix} \frac{g_{i}}{g_{t}} - \frac{g_{i}u^{2}}{6c_{s}^{2}} - \frac{g_{i}g_{t}u^{2}}{b}(H_{i} - u^{2}c_{s}^{2}) \\ \frac{g_{i}u}{3c_{s}^{2}} + \frac{2g_{i}g_{t}u}{b}(H_{i} - u^{2}c_{s}^{2}) \\ -\frac{g_{e}g_{i}}{g_{t}c_{s}^{2}} - \frac{6g_{e}g_{i}}{b}(H_{i} + 6g_{r}c_{s}^{2}) \\ -\frac{g_{i}^{2}}{g_{t}c_{s}^{2}} - \frac{6g_{i}}{b}(g_{i}H_{i} - g_{t}u^{2}c_{s}^{2}) \\ -\frac{g_{i}g_{r}}{g_{t}c_{s}^{2}} - \frac{6g_{i}g_{r}}{b}(H_{i} - 6g_{e}c_{s}^{2}) \end{pmatrix}, \quad \mathbf{L}_{4}(\mathbf{U}) = \begin{pmatrix} \frac{g_{r}}{g_{t}} - \frac{g_{r}u^{2}}{6c_{s}^{2}} - \frac{g_{r}g_{t}u^{2}}{b}(H_{r} - u^{2}c_{s}^{2}) \\ -\frac{g_{e}g_{r}}{3c_{s}^{2}} + \frac{2g_{r}g_{t}u}{b}(H_{r} - u^{2}c_{s}^{2}) \\ -\frac{g_{e}g_{r}}{g_{t}c_{s}^{2}} - \frac{6g_{e}g_{r}}{b}(H_{r} - 6g_{e}c_{s}^{2}) \\ -\frac{g_{i}g_{r}}{g_{t}c_{s}^{2}} - \frac{6g_{i}g_{r}}{b}(H_{r} + 6g_{e}c_{s}^{2}) \\ -\frac{g_{i}g_{r}}{g_{t}c_{s}^{2}} - \frac{6g_{r}}{b}(g_{r}H_{r} - g_{t}u^{2}c_{s}^{2}) \end{pmatrix},$$

$$(2.12)$$

$$\mathbf{L}_{5}(\mathbf{U}) = \frac{1}{12c_{s}^{2}} \begin{pmatrix} u(g_{t}u - 6c_{s}) \\ -2(g_{t}u - 3c_{s}) \\ 6g_{e} \\ 6g_{i} \\ 6g_{r} \end{pmatrix}.$$

To design a numerical method on the moving mesh, we rewrite the equations (2.6) in the reference frame of a moving control volume in the integral form as

$$\frac{d}{dt} \int_{\Omega(t)} \mathbf{U} d\Omega + \int_{\Gamma(t)} \mathbf{F} d\Gamma + \int_{\Omega(t)} \mathbf{N} d\Omega = \int_{\Gamma(t)} \mathbf{G} d\Gamma + \int_{\Omega(t)} \mathbf{S} d\Omega$$
 (2.13)

where $\Omega(t)$ is the moving control volume enclosed by its boundary $\Gamma(t)$. In the Lagrangian formulation, the vector of the evolving variables \mathbf{U} , the advection flux vector \mathbf{F} , the non-conservative advection term \mathbf{N} , the diffusion term \mathbf{G} and the energy-exchange terms \mathbf{S} are given by

$$\mathbf{U} = \begin{pmatrix} \rho \\ \rho u \\ E_e \\ E_i \\ E_r \end{pmatrix}, \quad \mathbf{F} = \begin{pmatrix} 0 \\ p_e u \\ p_i u \\ p_r u \end{pmatrix}, \quad \mathbf{N} = \begin{pmatrix} 0 \\ -\frac{1}{3}u\partial_x(2p_e - p_i - p_r) \\ -\frac{1}{3}u\partial_x(2p_i - p_e - p_r) \\ -\frac{1}{3}u\partial_x(2p_r - p_e - p_i) \end{pmatrix},$$

$$\mathbf{G} = \begin{pmatrix} 0 \\ 0 \\ \kappa_e \partial_x T_e \\ \kappa_i \partial_x T_i \\ \kappa_r \partial_x T_r^4 \end{pmatrix}, \quad \mathbf{S} = \begin{pmatrix} 0 \\ 0 \\ -\omega_{ei}(T_e - T_i) - \omega_{er}(T_e^4 - T_r^4) \\ \omega_{ei}(T_e - T_i) \\ \omega_{er}(T_e^4 - T_r^4) \end{pmatrix}. \quad (2.14)$$

Remark 2.1. For the purpose of designing the conservative scheme, we can distribute the kinetic energy arbitrarily among the three energy variables (with non-negative constant coefficients which sum to 1/2). The details of eigenvalues, eigenvectors etc. would change but all conclusions would stay the same. If we have some prior knowledge about typical sizes of the three internal energies e_e , e_r and e_i , we would probably want to choose the splitting coefficients of the kinetic energy in the same proportion. However, if we do not have such prior knowledge, an equal splitting as done here seems to be the most logical approach.

3 1D high order conservative Lagrangian scheme for the 3-T RH equations

3.1 High order spatial discretization

The spatial domain Ω is discretized into N computational cells $I_j = [x_{j-\frac{1}{2}}, x_{j+\frac{1}{2}}]$, the sizes of which are $\Delta x_j = x_{j+\frac{1}{2}} - x_{j-\frac{1}{2}}$ with j = 1, ..., N. The location of the cell center is denoted by x_j for a given cell I_j . The fluid velocity $u_{j-\frac{1}{2}}, j = 1, ..., N+1$ is defined at the nodes of the grid. All the variables solved directly are defined at the cell center x_j in the form of cell averages and this cell is their common control volume, that is,

$$\overline{\rho}_{j} = \frac{1}{\Delta x_{j}} \int_{I_{j}} \rho dx, \quad (\overline{\rho u})_{j} = \frac{1}{\Delta x_{j}} \int_{I_{j}} \rho u dx,$$

$$(\overline{E_{e}})_{j} = \frac{1}{\Delta x_{j}} \int_{I_{i}} E_{e} dx, \quad (\overline{E_{i}})_{j} = \frac{1}{\Delta x_{j}} \int_{I_{i}} E_{i} dx, \quad (\overline{E_{r}})_{j} = \frac{1}{\Delta x_{j}} \int_{I_{i}} E_{r} dx.$$

The finite volume explicit Lagrangian scheme with Euler forward time discretization for the system (2.13)-(2.14) can be written in the following form,

$$\overline{\mathbf{U}}_{j}^{n+1} \Delta x_{j}^{n+1} - \overline{\mathbf{U}}_{j} \Delta x_{j}
= \Delta t \left\{ -\left(\hat{\mathbf{F}}(\mathbf{U}_{j+\frac{1}{2}}^{-}, \mathbf{U}_{j+\frac{1}{2}}^{+}) - \hat{\mathbf{F}}(\mathbf{U}_{j-\frac{1}{2}}^{-}, \mathbf{U}_{j-\frac{1}{2}}^{+})\right) - \left(\overline{\mathbf{N}}_{j} \Delta x_{j} + [\mathbf{N}]_{j+\frac{1}{2}} + [\mathbf{N}]_{j-\frac{1}{2}}\right)
+ \left(\mathbf{G}(\mathbf{U}_{j+\frac{1}{2}}) - \mathbf{G}(\mathbf{U}_{j-\frac{1}{2}})\right) + \overline{\mathbf{S}}_{j} \Delta x_{j} \right\},$$
(3.1)

where $\overline{\mathbf{U}}_j, \overline{\mathbf{N}}_j, \overline{\mathbf{S}}_j$ are the cell averages of the vectors of $\mathbf{U}, \mathbf{N}, \mathbf{S}$ respectively. $[\mathbf{N}]_{j\pm 1/2}$ are the penalty jump terms for the discretization of the vector of \mathbf{N} . The superscript n+1 represents the values at the (n+1)-th time step. All the variables without the superscripts represent the values at the n-th time step. Δt is the n-th time step which will be determined by the stability conditions analyzed later. $\mathbf{U}_{j-\frac{1}{2}}^{\pm}, \mathbf{U}_{j+\frac{1}{2}}^{\pm}$ are the values of \mathbf{U} at the left and right sides of the cell boundary $x_{j-\frac{1}{2}}, x_{j+\frac{1}{2}}$ respectively. $\mathbf{U}_{j\pm 1/2}$ are the single values of \mathbf{U} at the cell boundary $x_{j\pm 1/2}$ respectively. In order to accomplish the high order spatial approximation, $\mathbf{U}_{j\pm 1/2}^{\pm}$ and $\mathbf{U}_{j\pm 1/2}$ are obtained from high order reconstructions which will be discussed

later. Since \mathbf{F} and \mathbf{G} are two different fluxes (advection and diffusion), $\mathbf{U}_{j\pm1/2}^{\pm}$ and $\mathbf{U}_{j\pm1/2}$, which serve the above two different fluxes, will be reconstructed in different ways. $\hat{\mathbf{F}}$ is the vector of the numerical fluxes for the advection terms across the cell boundary of $I_i(t)$, i.e.,

$$\hat{\mathbf{F}} = \left(\hat{F}_d, \hat{F}_m, \hat{F}_e, \hat{F}_i, \hat{F}_r\right)^T. \tag{3.2}$$

It should be determined in a suitable way to ensure upwinding and stability. It also should be consistent with the physical flux (2.14) in the sense that $\hat{\mathbf{F}}(\mathbf{U}, \mathbf{U}) = \mathbf{F}(\mathbf{U})$.

Next we will discuss the specific procedures to determine the individual terms in the Lagrangian scheme (3.1).

3.1.1 High order spatial discretization for the advection terms

We first discuss how to discretize the advection terms \mathbf{F} and \mathbf{N} in the equations (2.13)-(2.14).

I. Third order multi-resolution WENO reconstruction for the advection spatial discretization

To obtain a high order approximation to $U_{i\pm 1/2}^{\pm}$ used in the determination of the numerical flux $\hat{\mathbf{F}}$ and $\overline{\mathbf{N}}_j$ and $[\mathbf{N}]_{j\pm 1/2}$ in the scheme (3.1), we apply the multi-resolution WENO reconstruction [30] to reconstruct piecewise polynomial functions in each I_j by using the cellaverage information of the cell I_j and its neighbors, such that they are third order accurate approximations to the functions $\rho(x)$, $(\rho u)(x)$ $E_e(x)$, $E_i(x)$ and $E_r(x)$ in I_j respectively and also are essentially non-oscillatory near the discontinuities. The method of local characteristic decomposition is used in the procedure of the WENO reconstruction. We refer to [24] for the details of the similar Roe-type characteristic decomposition that we have used in this paper. In the multi-resolution WENO reconstruction, it chooses a series of unequal-sized hierarchical central spatial stencils to construct high-order and low-order polynomials on these stencils respectively. The final reconstruction polynomial is a linear combination of high-order and low-order polynomials with nonlinear weights. This type of WENO method can achieve optimal accuracy on the largest stencil in the smooth regions and can keep nonoscillatory behavior near discontinuities. The linear weights for such WENO reconstruction can be any fixed positive numbers on the condition that they sum to one, which is particularly suitable for moving meshes. This method can achieve arbitrarily high order accuracy. We will design a third order scheme as an example in this paper and the procedure of the third order multi-resolution WENO reconstruction in one-dimension consists of the following steps.

Step 1. We choose two central spatial stencils of different sizes. The small stencil is $R_1 = \{I_j\}$ and the large stencil is $R_2 = \{I_{j-1}, I_j, I_{j+1}\}$. We take the reconstruction of the first variable ϱ obtained by the local characteristic decomposition performed on $\overline{\mathbf{U}}$ as an example. For the first order approximation, we use R_1 to obtain $q_1(x) = \bar{\varrho}_j$. For the third order approximation, we use R_2 to obtain the quadratic polynomial $q_2(x) = a_0 + a_1(x - x_j) + a_2(x - x_j)^2$, where x_j is the coordinate of the center of I_j . Specifically, the coefficients $a_m, m = 0, 1, 2$ of $q_2(x)$ are determined by

$$\int_{I_k} q_2(x)dx = \overline{\varrho}_k \Delta x_k, k = j - 1, j, j + 1.$$
(3.3)

Step 2. Combine $q_1(x), q_2(x)$ with the linear weights. Take

$$p_1(x) = q_1(x),$$
 $p_2(x) = \frac{1}{\gamma_2}q_2(x) - \frac{\gamma_1}{\gamma_2}q_1(x)$

where γ_1, γ_2 are two linear weights which are defined as $\gamma_1 = \frac{1}{11}, \gamma_2 = \frac{10}{11}$ in our paper. We then have

$$\gamma_1 p_1(x) + \gamma_2 p_2(x) = q_2(x).$$

Step 3. Compute the smoothness indicators β_1 and β_2 , which measure how smooth the function $p_1(x)$ and $p_2(x)$ are in the cell I_j respectively.

Denote

$$\xi_{1} = |\overline{\varrho}_{j} - \overline{\varrho}_{j-1}|, \qquad \xi_{2} = |\overline{\varrho}_{j+1} - \overline{\varrho}_{j}|,
\overline{\zeta}_{1} = \begin{cases} 1, & \xi_{1} \geq \xi_{2} \\ 10, & otherwise \end{cases}, \quad \overline{\zeta}_{2} = 11 - \overline{\zeta}_{1},
\zeta_{1} = \frac{\overline{\zeta}_{1}}{\overline{\zeta}_{1} + \overline{\zeta}_{2}}, \qquad \zeta_{2} = 1 - \zeta_{1},
\sigma_{1} = \zeta_{1} \left(1 + \frac{|\xi_{1}^{2} - \xi_{2}^{2}|}{(\xi_{1} + \varepsilon)^{2}}\right), \qquad \sigma_{2} = \zeta_{2} \left(1 + \frac{|\xi_{1}^{2} - \xi_{2}^{2}|}{(\xi_{2} + \varepsilon)^{2}}\right), \qquad \sigma = \sigma_{1} + \sigma_{2}, \tag{3.4}$$

where ε is a small positive number to avoid the denominator of (3.4) to become zero. In the numerical tests of this paper, we choose $\varepsilon = 10^{-4}$. Then

$$\beta_1 = \frac{1}{\sigma^2} (\sigma_1(\overline{\varrho}_j - \overline{\varrho}_{j-1}) + \sigma_2(\overline{\varrho}_{j+1} - \overline{\varrho}_j))^2. \tag{3.5}$$

$$\beta_2 = \sum_{\alpha=1}^2 \int_{x_{j-\frac{1}{\alpha}}}^{x_{j+\frac{1}{2}}} (\Delta x_j)^{2\alpha-1} \left(\frac{d^\alpha p_2(x)}{dx^\alpha}\right)^2 dx. \tag{3.6}$$

Step 4. Compute the nonlinear weights based on the linear weights and the smoothness indicators, which follow the WENO-Z strategy as shown in [5]. The nonlinear weights are given as

$$w_l = \frac{\bar{w}_l}{\bar{w}_1 + \bar{w}_2}, \quad l = 1, 2,$$

where

$$\bar{w}_l = \gamma_l \left(1 + \frac{\tau}{(\beta_l + \varepsilon)^2} \right), \quad \tau = (\beta_2 - \beta_1)^2, \quad l = 1, 2.$$

Step 5. The final reconstruction polynomial for the cell I_i is given by

$$\varrho_i(x) = w_1 p_1(x) + w_2 p_2(x).$$

II. The HLLC flux for the conservative advection term in 3-T equations in the Lagrangian formulation

In this part, we will discuss how to determine the numerical flux $\hat{\mathbf{F}}$ (3.2) in the scheme (3.1). We consider the following three-temperature equations which only include the conservative advection terms,

$$\partial_t \mathbf{U} + \partial_x \mathbf{F} = 0 \tag{3.7}$$

where

$$\mathbf{U} = \begin{pmatrix} \rho \\ \rho u \\ E_e \\ E_i \\ E_r \end{pmatrix}, \qquad \mathbf{F} = \begin{pmatrix} \rho u \\ \rho u^2 + p \\ (E_e + p_e)u \\ (E_i + p_i)u \\ (E_r + p_r)u \end{pmatrix}, \tag{3.8}$$

where $p = p_e + p_i + p_r$. We want to design a HLLC flux for the Lagrangian scheme solving (3.7)-(3.8), which is derived from the divergence theorem (critical for the proof of positivity-preserving property discussed in the next section) and is suitable for multi-material problems.

Since in the Lagrangian formulation, the flux for the first equation of (3.7) is zero (see (2.14)), we should set

$$\hat{F}_d = 0. (3.9)$$

For the HLLC flux, two averaged intermediate states \mathbf{U}_L^* and \mathbf{U}_R^* between the two acoustic waves s_L , s_R are considered, which are separated by the contact wave (interface) with the velocity s_* , see Fig. 3.1. From the definition of HLLC, we have

$$s_* = \frac{\hat{F}_e + \hat{F}_i + \hat{F}_r}{\hat{F}_m}. (3.10)$$

Apply the divergence theorem in the left region ABCD and the right region DCEF (Fig. 3.1) for the Riemann problem respectively, then we obtain

$$\mathbf{U}_{L}^{*}(s_{*}-s_{L}) = -\mathbf{U}_{L}s_{L} + \mathbf{F}(\mathbf{U}_{L}) - \hat{\mathbf{F}}, \tag{3.11}$$

$$\mathbf{U}_{R}^{*}(s_{R} - s_{*}) = \mathbf{U}_{R}s_{R} - \mathbf{F}(\mathbf{U}_{R}) + \hat{\mathbf{F}}, \tag{3.12}$$

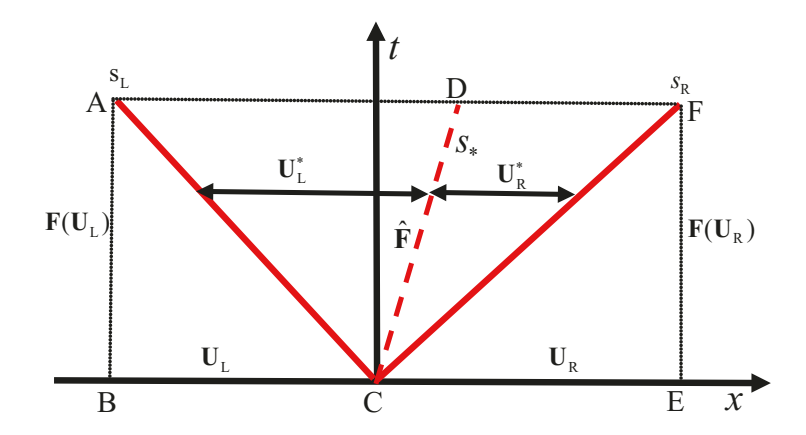


Figure 3.1: Simplified Riemann fan for the HLLC flux.

where

$$\mathbf{U}_{L} = \begin{pmatrix} \rho_{L} \\ \rho_{L} u_{L} \\ E_{e,L} \\ E_{r,L} \end{pmatrix}, \qquad \mathbf{U}_{R} = \begin{pmatrix} \rho_{R} \\ \rho_{R} u_{R} \\ E_{e,R} \\ E_{i,R} \\ E_{r,R} \end{pmatrix}, \\
\mathbf{U}_{L}^{*} = \begin{pmatrix} \rho_{L}^{*} \\ \rho_{L}^{*} u_{L}^{*} \\ E_{e,L}^{*} \\ E_{i,L}^{*} \\ E_{r,L}^{*} \end{pmatrix}, \qquad \mathbf{U}_{R}^{*} = \begin{pmatrix} \rho_{R}^{*} \\ \rho_{R}^{*} u_{R}^{*} \\ E_{e,R}^{*} \\ E_{e,R}^{*} \\ E_{i,R}^{*} \\ E_{r,R}^{*} \end{pmatrix}. \tag{3.13}$$

Suppose the velocity and pressure of electron, ion and radiation are constant in the two middle regions of HLLC, denoted as $u^*(=u_L^*=u_R^*), p_e^*, p_i^*, p_r^*$. For simplicity in the form, here we consider the γ -law equation of state for both electron and ion and suppose they have the same value denoted as γ_L and γ_R in the left and right initial regions respectively. Then we have,

$$\mathbf{U}_{L}^{*} = \begin{pmatrix} \rho_{L}^{*} \\ \rho_{L}^{*}u^{*} \\ \frac{p_{e}^{*}}{\gamma_{L}-1} + \frac{1}{6}\rho_{L}^{*}(u^{*})^{2} \\ \frac{p_{i}^{*}}{\gamma_{L}-1} + \frac{1}{6}\rho_{L}^{*}(u^{*})^{2} \\ 3p_{r}^{*} + \frac{1}{6}\rho_{L}^{*}(u^{*})^{2} \end{pmatrix}, \quad \mathbf{U}_{R}^{*} = \begin{pmatrix} \rho_{R}^{*} \\ \rho_{R}^{*}u^{*} \\ \frac{p_{e}^{*}}{\gamma_{R}-1} + \frac{1}{6}\rho_{R}^{*}(u^{*})^{2} \\ \frac{p_{i}^{*}}{\gamma_{R}-1} + \frac{1}{6}\rho_{R}^{*}(u^{*})^{2} \\ 3p_{r}^{*} + \frac{1}{6}\rho_{R}^{*}(u^{*})^{2} \end{pmatrix}.$$
(3.14)

Substitute (3.13) and (3.14) into (3.11), from the first two formulas of (3.11), we get,

$$\rho_L^* = \frac{\rho_L(u_L - s_L)}{(s_* - s_L)}, \qquad \rho_R^* = \frac{\rho_R(s_R - u_R)}{(s_R - s_*)},
u^* = \frac{\rho_L u_L(u_L - s_L) + \rho_R u_R(s_R - u_R) + p_L - p_R}{\rho_L(u_L - s_L) + \rho_R(s_R - u_R)},
\hat{F}_m = \rho_L(u_L - u^*)(u_L - s_L) + p_L.$$
(3.15)

Sum the third formula of (3.11) and (3.12), similarly to the fourth and fifth formulas, then we get,

$$p_{e}^{*} = \frac{(\gamma_{L} - 1)(\gamma_{R} - 1)q_{e}}{(\gamma_{R} - 1)(s_{*} - s_{L}) + (\gamma_{L} - 1)(s_{R} - s_{*})},$$

$$p_{i}^{*} = \frac{(\gamma_{L} - 1)(\gamma_{R} - 1)q_{i}}{(\gamma_{R} - 1)(s_{*} - s_{L}) + (\gamma_{L} - 1)(s_{R} - s_{*})},$$

$$p_{r}^{*} = \frac{q_{r}}{3(s_{R} - s_{L})},$$
(3.16)

where

$$q_{e} = E_{e,L}(u_{L} - s_{L}) + E_{e,R}(s_{R} - u_{R}) + p_{e,L}u_{L} - p_{e,R}u_{R} - \frac{1}{6}(\rho_{L}(u_{L} - s_{L}) + \rho_{R}(s_{R} - u_{R}))(u^{*})^{2},$$

$$q_{i} = E_{i,L}(u_{L} - s_{L}) + E_{i,R}(s_{R} - u_{R}) + p_{i,L}u_{L} - p_{i,R}u_{R} - \frac{1}{6}(\rho_{L}(u_{L} - s_{L}) + \rho_{R}(s_{R} - u_{R}))(u^{*})^{2},$$

$$q_{r} = E_{r,L}(u_{L} - s_{L}) + E_{r,R}(s_{R} - u_{R}) + p_{r,L}u_{L} - p_{r,R}u_{R} - \frac{1}{6}(\rho_{L}(u_{L} - s_{L}) + \rho_{R}(s_{R} - u_{R}))(u^{*})^{2}.$$

$$(3.17)$$

Sum the last three formulas of (3.11) and (3.12) respectively, and using (3.10) we get,

$$\left(\frac{p_e^* + p_i^*}{\gamma_L - 1} + 3p_r^*\right)(s_* - s_L) = -\hat{F}_m s_* + b_L,
\left(\frac{p_e^* + p_i^*}{\gamma_R - 1} + 3p_r^*\right)(s_R - s_*) = \hat{F}_m s_* + b_R,$$
(3.18)

where

$$b_L = p_L u_L + (u_L - s_L)(E_L - \frac{1}{2}\rho_L(u^*)^2),$$

$$b_R = -p_R u_R + (s_R - u_R)(E_R - \frac{1}{2}(\rho_R(u^*)^2).$$

Substitute p_e^*, p_i^*, p_r^* by (3.16) into (3.18), then we obtain the following relationship for s_* ,

$$\left(\frac{(\gamma_R - 1)(q_e + q_i)}{(\gamma_R - 1)(s_* - s_L) + (\gamma_L - 1)(s_R - s_*)} + \frac{q_r}{s_R - s_L}\right)(s_* - s_L) = -\hat{F}_m s_* + b_L. \tag{3.19}$$

If $\gamma_R = \gamma_L$, then

$$s_* = \frac{s_L(q_e + q_i + q_r) + b_L(s_R - s_L)}{q_e + q_i + q_r + \hat{F}_m(s_R - s_L)}.$$
(3.20)

If $\gamma_R \neq \gamma_L$, then

$$s_* = \frac{d_1 + \sqrt{d_2}}{2(\gamma_R - \gamma_L)(q_r + \hat{F}_m(s_R - s_L))},$$
(3.21)

where

$$d_1 = \hat{F}_m \left((\gamma_L + \gamma_R - 2) s_L s_R - (\gamma_R - 1) s_L^2 - (\gamma_L - 1) s_R^2 \right) + b_L (s_R - s_L) (\gamma_R - \gamma_L)$$

$$-(q_e + q_i)(s_R - s_L)(\gamma_R - 1) + q_r \left(s_L(2\gamma_R - \gamma_L - 1) - s_R(\gamma_L - 1)\right),$$

$$d_2 = \left(\hat{F}_m(s_L^2(\gamma_R - 1) + s_R^2(\gamma_L - 1) - s_L s_R(\gamma_L + \gamma_R - 2)\right) - b_L(s_R - s_L)(\gamma_R - \gamma_L) \qquad (3.22)$$

$$+(q_e + q_i)(s_R - s_L)(\gamma_R - 1) + q_r \left(-s_L(2\gamma_R - \gamma_L - 1) + s_R(\gamma_L - 1)\right)\right)^2 - 4\left(q_r(\gamma_R - \gamma_L)\right)$$

$$+\hat{F}_m(\gamma_R - \gamma_L)(s_R - s_L)\left(b_L(s_L s_R(\gamma_L + \gamma_R - 2) - s_L^2(\gamma_R - 1) - s_R^2(\gamma_L - 1)\right)$$

$$-(q_e + q_i + q_r)s_L(s_R - s_L)(\gamma_R - 1) + q_r s_L s_R(\gamma_R - \gamma_L)\right).$$

We can check that $s_* \in [s_L, s_R]$.

After we obtain s_* , then from (3.11) we can determine the HLLC numerical flux for the 3-T RH equations (3.7)-(3.8),

$$\begin{cases}
\hat{F}_{d} = 0, \\
\hat{F}_{m} = \rho_{L}(u_{L} - u^{*})(u_{L} - s_{L}) + p_{L}, \\
\hat{F}_{e} = -\frac{p_{e}^{*}}{\gamma_{L} - 1}(s_{*} - s_{L}) + (E_{e,L} - \frac{1}{6}\rho_{L}(u^{*})^{2})(u_{L} - s_{L}) + p_{e,L}u_{L}, \\
\hat{F}_{i} = -\frac{p_{i}^{*}}{\gamma_{L} - 1}(s_{*} - s_{L}) + (E_{i,L} - \frac{1}{6}\rho_{L}(u^{*})^{2})(u_{L} - s_{L}) + p_{i,L}u_{L}, \\
\hat{F}_{r} = -3p_{r}^{*}(s_{*} - s_{L}) + (E_{r,L} - \frac{1}{6}\rho_{L}(u^{*})^{2})(u_{L} - s_{L}) + p_{r,L}u_{L},
\end{cases} (3.23)$$

which is under the assumption that both electron and ion satisfy the γ -law equation of states and their values of γ are the same. For the case $\gamma_e \neq \gamma_i$, similar analysis can be made, but the form of the numerical flux is more complicated. In principle, we can derive the HLLC solver for the non- γ -law case in a similar way, however the algebra will be much more involved.

III. The determination of the nonconservative advection terms

The non-conservative terms $\overline{\mathbf{N}}_j$, $[\mathbf{N}]_{j+\frac{1}{2}}$, $[\mathbf{N}]_{j-\frac{1}{2}}$ in the scheme (3.1) are determined following the strategy for solving Hamilton-Jacobi equations [12], which is also used in [21] to discretize the non-conservative terms in the Godunov form of MHD and is equivalent to a specific form of the usual path-conservative strategy. For our case, it is given by

$$\overline{\mathbf{N}}_{j} = \begin{pmatrix}
0 \\
0 \\
-\sum_{g=1}^{N_{g}} \frac{1}{3} \omega_{g} u_{g} (2(p_{e})_{x,g} - (p_{i})_{x,g} - (p_{r})_{x,g}) \Delta x_{j} \\
-\sum_{g=1}^{N_{g}} \frac{1}{3} \omega_{g} u_{g} (2(p_{i})_{x,g} - (p_{e})_{x,g} - (p_{r})_{x,g}) \Delta x_{j} \\
-\sum_{g=1}^{N_{g}} \frac{1}{3} \omega_{g} u_{g} (2(p_{r})_{x,g} - (p_{e})_{x,g} - (p_{i})_{x,g}) \Delta x_{j}
\end{pmatrix} := \begin{pmatrix}
0 \\
\overline{N}_{j,e} \\
\overline{N}_{j,i} \\
\overline{N}_{j,r}
\end{pmatrix}$$
(3.24)

$$[\mathbf{N}]_{j+\frac{1}{2}} + [\mathbf{N}]_{j-\frac{1}{2}} = \begin{pmatrix} 0 \\ \max\{-\frac{1}{3}u_{j-\frac{1}{2}}, 0\}[2p_e - p_i - p_r]_{j-\frac{1}{2}} + \min\{-\frac{1}{3}u_{j+\frac{1}{2}}, 0\}[2p_e - p_i - p_r]_{j+\frac{1}{2}} \\ \max\{-\frac{1}{3}u_{j-\frac{1}{2}}, 0\}[2p_i - p_e - p_r]_{j-\frac{1}{2}} + \min\{-\frac{1}{3}u_{j+\frac{1}{2}}, 0\}[2p_i - p_e - p_r]_{j+\frac{1}{2}} \\ \max\{-\frac{1}{3}u_{j-\frac{1}{2}}, 0\}[2p_r - p_e - p_i]_{j-\frac{1}{2}} + \min\{-\frac{1}{3}u_{j+\frac{1}{2}}, 0\}[2p_r - p_e - p_i]_{j+\frac{1}{2}} \end{pmatrix}$$
 (3.25)

$$:= \begin{pmatrix} 0 \\ 0 \\ [N]_{j,e} \\ [N]_{j,i} \\ [N]_{j,r} \end{pmatrix}$$

where g is denoted to be the Gaussian points in the cell I_j , N_g is the number of Gaussian points. In order to achieve third order accuracy, we choose g=2, the coordinates of the two Gaussian points are $x_j \pm \frac{\sqrt{3}\Delta x_j}{6}$. $(p_e)_{x,g}, (p_i)_{x,g}, (p_r)_{x,g}$ are determined by the values and the derivative values of the reconstruction polynomials of U at the Gaussian points g, that is,

$$(p_e)_x = (\gamma_e - 1) \left((E_e)_x - \frac{(\rho u)(\rho u)_x}{3\rho} + \frac{(\rho u)^2 \rho_x}{6\rho^2} \right),$$

$$(p_i)_x = (\gamma_i - 1) \left((E_i)_x - \frac{(\rho u)(\rho u)_x}{3\rho} + \frac{(\rho u)^2 \rho_x}{6\rho^2} \right),$$

$$(p_r)_x = (\gamma_r - 1) \left((E_r)_x - \frac{(\rho u)(\rho u)_x}{3\rho} + \frac{(\rho u)^2 \rho_x}{6\rho^2} \right).$$
(3.26)

 $[p_e]_{j\pm\frac{1}{2}} = (p_e)_{j\pm\frac{1}{2}}^+ - (p_e)_{j\pm\frac{1}{2}}^-, [p_i]_{j\pm\frac{1}{2}} = (p_i)_{j\pm\frac{1}{2}}^+ - (p_i)_{j\pm\frac{1}{2}}^-, [p_r]_{j\pm\frac{1}{2}} = (p_r)_{j\pm\frac{1}{2}}^+ - (p_r)_{j\pm\frac{1}{2}}^-, [p_e]_{j\pm\frac{1}{2}}^\pm, (p_r)_{j\pm\frac{1}{2}}^\pm, (p_r)_{j\pm\frac{1}{2}}^\pm, (p_r)_{j\pm\frac{1}{2}}^\pm$ are determined by $\mathbf{U}_{j\pm\frac{1}{2}}^\pm$ from the reconstruction polynomials in the two neighboring cells.

3.1.2 The determination of the nodal velocity

The fluid velocity $u_{j-\frac{1}{2}}$ at each node is determined by

$$u_{j-\frac{1}{2}} = (s_*)_{j-\frac{1}{2}}, \quad j = 1, ..., N+1,$$
 (3.27)

where $(s_*)_{j-\frac{1}{2}}$ is given by (3.20) or (3.21). Then the mesh moves according to the following formula,

$$x_{j-\frac{1}{2}}^{n+1} = x_{j-\frac{1}{2}} + u_{j-\frac{1}{2}} \Delta t, \quad j = 1, ..., N+1,$$
 (3.28)

if the Euler forward time discretization is considered.

3.1.3 The determination of the energy-exchange terms

The terms of $\overline{\mathbf{S}}_i$ in the scheme (3.1) are determined by

$$\overline{\mathbf{S}}_{j} = \begin{pmatrix}
0 & 0 \\
-\sum_{g=1}^{N_{g}} \left((\omega_{ei})_{g}((T_{e})_{g} - (T_{i})_{g}) + (\omega_{er})_{g}((T_{e}^{4})_{g} - (T_{r}^{4})_{g}) \right) \\
\sum_{g=1}^{N_{g}} (\omega_{ei})_{g}((T_{e})_{g} - (T_{i})_{g}) \\
\sum_{g=1}^{N_{g}} (\omega_{er})_{g}((T_{e}^{4})_{g} - (T_{r}^{4})_{g})
\end{pmatrix} := \begin{pmatrix}
0 \\
0 \\
\overline{S}_{j,e} \\
\overline{S}_{j,i} \\
\overline{S}_{j,r}
\end{pmatrix} (3.29)$$

where $(T_e)_g$, $(T_i)_g$, $(T_r)_g$ and $(\omega_{ei})_g$, $(\omega_{er})_g$ are the values of the related variables at the Gaussian points which are obtained from the reconstruction polynomials of **U** introduced in the above subsection. g, N_g have the same definition as those in the above subsection.

3.1.4 High order spatial discretization for the diffusion terms

Next we discuss how to discretize the diffusion terms G in the scheme (3.1).

I. Fourth order multi-resolution WENO reconstruction for the diffusion spatial discretization

To obtain a fourth order approximation to $U_{j\pm 1/2}$ used in the diffusion flux G, take ρ as an example, the specific procedures for the multi-resolution WENO interpolation is as follows.

Step 1. To reconstruct the values of **U** and its derivatives at $x_{j-\frac{1}{2}}$, we choose two spatial stencils of different sizes. One small stencil is $T_1 = \{I_{j-1}, I_j\}$ to reconstruct a linear polynomial $q_1(x) = a_0^1 + a_1^1(x - x_{j-\frac{1}{2}})$. One large stencil is $T_2 = \{I_{j-2}, I_{j-1}, I_j, I_{j+1}\}$, which is used to reconstruct a cubic polynomial $q_2(x) = a_0^2 + a_1^2(x - x_{j-\frac{1}{2}}) + a_2^2(x - x_{j-\frac{1}{2}})^2 + a_3^2(x - x_{j-\frac{1}{2}})^3$. We adopt the similar way as (3.3) used in the advection term to determine the coefficients of the above polynomials.

Step 2. Combine $q_1(x), q_2(x)$ with the linear weights. Take

$$p_1(x) = q_1(x),$$
 $p_2(x) = \frac{1}{\gamma_2}q_2(x) - \frac{\gamma_1}{\gamma_2}q_1(x)$

where $\gamma_1 = \frac{1}{11}$, $\gamma_2 = \frac{10}{11}$ are the linear weights. It could make sure

$$\gamma_1 p_1(x) + \gamma_2 p_2(x) = q_2(x).$$

Step 3. Compute the smoothness indicators β_l , l=1,2, which measure how smooth the function $p_1(x)$ and $p_2(x)$ are at $x_{j-\frac{1}{2}}$ respectively.

$$\beta_2 = \sum_{\alpha=2}^{3} \int_{x_{j-1}}^{x_j} (x_j - x_{j-1})^{2\alpha - 1} \left(\frac{d^{\alpha} p_2(x)}{dx^{\alpha}}\right)^2 dx.$$
 (3.30)

If the formula (3.30) is adopted to compute β_1 , then $\beta_1 = 0$. To avoid this, we introduce extra two small stencils as $T_3 = \{I_{j-2}, I_{j-1}, I_j\}$ and $T_4 = \{I_{j-1}, I_j, I_{j+1}\}$ to reconstruct two quadratic polynomials $q_3(x) = a_0^3 + a_1^3(x - x_{j-\frac{1}{2}}) + a_2^3(x - x_{j-\frac{1}{2}})^2$, $q_4(x) = a_0^4 + a_1^4(x - x_{j-\frac{1}{2}}) + a_2^4(x - x_{j-\frac{1}{2}})^2$. Then,

$$\xi_1 = \int_{x_{j-1}}^{x_j} (x_j - x_{j-1})^3 \left(\frac{d^2 q_3(x)}{dx^2}\right)^2 dx, \quad \xi_2 = \int_{x_{j-1}}^{x_j} (x_j - x_{j-1})^3 \left(\frac{d^2 q_4(x)}{dx^2}\right)^2 dx, \quad (3.31)$$

$$\beta_1 = \min\{\xi_1, \xi_2\}. \tag{3.32}$$

Step 4. Compute the nonlinear weights based on the linear weights and the smoothness indicators. The nonlinear weights are given as

$$w_l = \frac{\bar{w}_l}{\bar{w}_1 + \bar{w}_2}, \quad \bar{w}_l = \gamma_l \left(1 + \frac{\tau}{(\beta_l + \varepsilon)^2} \right), \quad l = 1, 2,$$

where $\varepsilon = 10^{-4}$ and $\tau = (\beta_2 - \beta_1)^2$.

Step 5. The final interpolation polynomial at the cell boundary $x_{j-\frac{1}{2}}$ is given by

$$\rho_{j-\frac{1}{2}}(x) = w_1 p_1(x) + w_2 p_2(x).$$

The other variables of U can be obtained in the similar way. Notice that in the WENO reconstruction for the diffusion term, the characteristic decomposition is not needed.

II. The determination of the diffusion terms

We use the following formulas to determine $(T_e)_x$, $(T_i)_x$, $(T_r^4)_x$ in the diffusion terms \mathbf{G} ,

$$(T_e)_x = \frac{1}{c_{ve}\rho^2} \left(\rho(E_e)_x - E_e\rho_x - \frac{\rho u(\rho u)_x}{3} + \frac{(\rho u)^2 \rho_x}{3\rho} \right),$$

$$(T_i)_x = \frac{1}{c_{vi}\rho^2} \left(\rho(E_i)_x - E_i\rho_x - \frac{\rho u(\rho u)_x}{3} + \frac{(\rho u)^2 \rho_x}{3\rho} \right),$$

$$(T_r^4)_x = \frac{1}{a} \left((E_r)_x - \frac{\rho u(\rho u)_x}{3\rho} + \frac{(\rho u)^2 \rho_x}{6\rho^2} \right),$$
(3.33)

where $\{\rho, \rho u, E_e, E_i, E_r\}$ and their derivatives are obtained by the above fourth order multiresolution WENO reconstruction.

3.1.5 The conservation property of the scheme

For the scheme (3.1), we can prove that it can keep the conservation of mass, momentum and total energy if all the terms in (3.1) are discretized in a compatible way and the periodic or zero-flux boundary conditions are considered, the proof on the conservation of mass, momentum is trivial. For the conservation of total energy $E = E_e + E_i + E_r$, we can prove it as follows.

Sum the last three equations of the scheme (3.1) and notice that $\bar{N}_{j,e} + \bar{N}_{j,i} + \bar{N}_{j,r} = 0$, $[N]_{j,e} + [N]_{j,i} + [N]_{j,r} = 0$ and $\bar{S}_{j,e} + \bar{S}_{j,i} + \bar{S}_{j,r} = 0$, then we have

$$\sum_{j=1}^{N} \left[\overline{E}_{e,j}^{n+1} + \overline{E}_{i,j}^{n+1} + \overline{E}_{r,j}^{n+1} \right] - \sum_{j=1}^{N} \left[\overline{E}_{e,j} + \overline{E}_{i,j} + \overline{E}_{r,j} \right] = 0$$
(3.34)

which implies

$$\sum_{j=1}^{N} \overline{E}_j^{n+1} = \sum_{j=1}^{N} \overline{E}_j. \tag{3.35}$$

3.2 The high order Runge-Kutta time discretization

To design a Lagrangian scheme with uniformly third order accuracy both in space and time, the time marching is implemented by a third order total variation diminishing (TVD), or strong stability preserving (SSP) Runge-Kutta type method [23, 18], which has the following form in the Lagrangian formulation [7].

Stage 1,

$$x_{j-\frac{1}{2}}^{(1)} = x_{j-\frac{1}{2}} + \Delta t u_{j-\frac{1}{2}},$$

$$\overline{\mathbf{U}}_{j}^{(1)} \Delta x_{j}^{(1)} = \overline{\mathbf{U}}_{j} \Delta x_{j} + \Delta t \mathbf{L}(\overline{\mathbf{U}}_{j});$$
(3.36)

Stage 2,

$$x_{j-\frac{1}{2}}^{(2)} = x_{j-\frac{1}{2}}^{(1)} + \frac{1}{4}\Delta t \left[-3u_{j-\frac{1}{2}} + u_{j-\frac{1}{2}}^{(1)} \right],$$

$$\overline{\mathbf{U}}_{j}^{(2)} \Delta x_{j}^{(2)} = \overline{\mathbf{U}}_{j}^{(1)} \Delta x_{j}^{(1)} + \frac{1}{4}\Delta t \left(-3\mathbf{L}(\overline{\mathbf{U}}_{j}) + \mathbf{L}(\overline{\mathbf{U}}_{j}^{(1)}) \right);$$
(3.37)

Stage 3,

$$x_{j-\frac{1}{2}}^{n+1} = x_{j-\frac{1}{2}} + \frac{1}{6}\Delta t \left(u_{j-\frac{1}{2}} + u_{j-\frac{1}{2}}^{(1)} + 4u_{j-\frac{1}{2}}^{(2)} \right),$$

$$\overline{\mathbf{U}}_{j}^{n+1} \Delta x_{j}^{n+1} = \overline{\mathbf{U}}_{j} \Delta x_{j} + \frac{1}{6}\Delta t \left(\mathbf{L}(\overline{\mathbf{U}}_{j}) + \mathbf{L}(\overline{\mathbf{U}}_{j}^{(1)}) + 4\mathbf{L}(\overline{\mathbf{U}}_{j}^{(2)}) \right); \tag{3.38}$$

where L is the numerical spatial operator representing the right hand of the scheme (3.1).

3.3 The time step for the Lagrangian scheme solving the 3-T RH equations

For the explicit Lagrangian scheme (3.1), the time step is limited by the three terms coming from the 3-T RH equations, namely, the advection term, the diffusion term and the energy-exchange term.

We rewrite the system (2.1) in the following form,

$$\frac{\partial \mathbf{U}}{\partial t} + A \frac{\partial \mathbf{U}}{\partial x} = \frac{\partial (B \frac{\partial \mathbf{U}}{\partial x})}{\partial x} + S(\mathbf{U})$$
(3.39)

where $\mathbf{U} = (\rho, \rho u, E_e, E_i, E_r)^T$. The matrix A is defined as (2.8).

Denote

$$\tilde{e}_e = e_e - \frac{1}{6}u^2, \, \tilde{e}_i = E_i - \frac{1}{6}u^2,$$
(3.40)

Then the Jacobian matrix B related to the diffusion term can be represented as,

$$B = \begin{pmatrix} 0 & 0 & 0 & 0 & 0 \\ 0 & 0 & 0 & 0 & 0 \\ -\frac{\kappa_e \tilde{e}_e}{c_{ve} \rho} & -\frac{\kappa_e u}{3c_{ve} \rho} & \frac{\kappa_e}{c_{ve} \rho} & 0 & 0 \\ -\frac{\kappa_i \tilde{e}_i}{c_{vi} \rho} & -\frac{\kappa_i u}{3c_{vi} \rho} & 0 & \frac{\kappa_i}{c_{vi} \rho} & 0 \\ \frac{\kappa_r u^2}{6a} & -\frac{\kappa_r u}{3a} & 0 & 0 & \frac{\kappa_r}{a} \end{pmatrix}.$$
 (3.41)

Its eigenvalues are listed as follows,

$$\{0, 0, \frac{\kappa_e}{c_{ve}\rho}, \frac{\kappa_i}{c_{vi}\rho}, \frac{\kappa_r}{a}\}. \tag{3.42}$$

Its eigenvalues are in the following,

$$\{0, 0, 0, \alpha_1, \alpha_2\}, \tag{3.44}$$

where

$$\alpha_1 = \frac{-s_1 + s_2}{s}, \quad \alpha_2 = \frac{s_1 + s_2}{s}$$
 (3.45)

with

$$s_{1} = \sqrt{\left(a\omega_{ei}c_{ve}^{4} + a\omega_{ei}c_{ve}^{3}c_{vi} + 4a\omega_{er}c_{vi}e_{e}^{3} + \omega_{er}c_{ve}^{4}c_{vi}\rho\right)^{2} - 4a\omega_{ei}\omega_{er}c_{ve}^{4}c_{vi}\left(4ae_{e}^{3} + c_{ve}^{4}\rho + c_{ve}^{3}c_{vi}\rho\right)},$$

$$s_{2} = -\left(a\omega_{ei}c_{ve}^{4} + a\omega_{ei}c_{ve}^{3}c_{vi} + 4a\omega_{er}c_{vi}e_{e}^{3} + \omega_{er}c_{ve}^{4}c_{vi}\rho\right),$$

$$s = 2ac_{ve}^{4}c_{vi}\rho.$$

The time step is limited by the above three terms as

$$\Delta t_{eq} \le \min_{j=1,\dots,N} \frac{\lambda}{\nu_j}, \qquad \nu_j = \frac{(c_s)_j}{\Delta x_j} + \frac{2d_j}{\Delta x_i^2} + s_j \tag{3.46}$$

where $(c_s)_j$ is defined by (2.10). λ is a positive constant less than 1, which is chosen as 0.5 in this paper.

$$d_j = \max\{\frac{\kappa_e}{c_{ve}\rho_j}, \frac{\kappa_i}{c_{vi}\rho_j}, \frac{\kappa_r}{a}\}, \quad s_j = \max\{|(\alpha_1)_j|, |(\alpha_2)_j|\}.$$
(3.47)

To avoid the grid from interacting within the time step, we also need the time step to satisfy

$$\Delta t_{grid} = \mu \min_{j=1,\dots,N+1} \left\{ \min(\Delta x_{j-1}, \Delta x_j) / u_{j-\frac{1}{2}} \right\}, \tag{3.48}$$

where μ is a constant which is chosen as 0.45 in this paper.

Then the final time step Δt is determined by the following formula,

$$\Delta t = \min\{\Delta t_{ea}, \Delta t_{arid}\}. \tag{3.49}$$

4 The positivity-preserving issue on the Lagrangian scheme solving the 3-T RH equations (3.7)-(3.8)

4.1 The first order positivity-preserving Lagrangian scheme for the 3-T RH equations (3.7)-(3.8)

The system (2.13)-(2.14) includes the nonlinear advection, diffusion and source terms. We are unable to analyze the positivity-preserving property of the full system so far. But for the simpler form (3.7)-(3.8) which only contains the conservative advection term in space, we can prove the following first order Lagrangian scheme with the HLLC flux (3.23) can keep the positivity-preserving property under certain conditions

$$\overline{\mathbf{U}}_{j}^{n+1} \Delta x_{j}^{n+1} - \overline{\mathbf{U}}_{j} \Delta x_{j} = -\Delta t \left(\hat{\mathbf{F}} (\overline{\mathbf{U}}_{j}, \overline{\mathbf{U}}_{j+1}) - \hat{\mathbf{F}} (\overline{\mathbf{U}}_{j-1}, \overline{\mathbf{U}}_{j}) \right), \tag{4.1}$$

where $\hat{\mathbf{F}}$ is defined by (3.23).

Define the set of admissible states by

$$G = \left\{ \mathbf{U} = (\rho, \rho u, E_e, E_i, E_r)^T, \quad \rho > 0, \quad e_e > 0, \quad e_i > 0, \quad e_r > 0 \right\}.$$
 (4.2)

Lemma: The set of admissible states G is a convex set for the γ -law EOS given by (2.3). **Proof.** Denote $\check{e}_e = \rho e_e, \check{e}_i = \rho e_i, \check{e}_r = \rho e_r$. It can be easily verified that $\check{e}_e, \check{e}_i, \check{e}_r$ are concave functions of $\mathbf{U} = (\rho, \rho u, E_e, E_i, E_r)^T$ if $\rho > 0$. Using Jensen's inequality, we have

$$\check{e}_e(d\mathbf{U}_1 + (1-d)\mathbf{U}_2) \ge d\check{e}_e(\mathbf{U}_1) + (1-d)\check{e}_e(\mathbf{U}_2), \quad if \quad \rho_1 \ge 0, \quad \rho_2 \ge 0,$$

for $\mathbf{U}_1 = (\rho_1, (\rho u)_1, (E_e)_1, (E_i)_1, (E_r)_1)^T$, $\mathbf{U}_2 = (\rho_2, (\rho u)_2, (E_e)_2, (E_i)_2, (E_r)_2)^T$ and $0 \le d \le 1$. Similar proof could be done for \check{e}_i and \check{e}_r . Thus G is a convex set.

The scheme (4.1) is called positivity-preserving if $\{\overline{\mathbf{U}}_j \in G, j=1,...,N\}$ implies $\{\overline{\mathbf{U}}_j^{n+1} \in G, j=1,...,N\}$. Following the design of the HLLC flux, the divergence theorem is satisfied exactly in the two regions ABCD and DCEF respectively in Figure 3.1, and also u^*, p_e^*, p_i^*, p_r^* are continuous along the contact line (CD). Meanwhile, by choosing a suitable CFL condition, the two waves in Figure 4.1 centered at $x_{j-\frac{1}{2}}$ and at $x_{j+\frac{1}{2}}$ do not interact within the time step Δt . In this case, $\overline{\mathbf{U}}_j^{n+1}$ in the scheme (4.1) can be described as the exact integration of the approximate Riemann solver over $[x_{j-\frac{1}{2}}^{n+1}, x_{j+\frac{1}{2}}^{n+1}]$ which can be broken into two parts (see Figure 4.1), that is,

$$\overline{\mathbf{U}}_{j}^{n+1} = \frac{1}{\Delta x_{j}^{n+1}} \int_{x_{j-\frac{1}{2}}^{n+1}}^{x_{j}^{n+1}} R(x/t, \overline{\mathbf{U}}_{j-1}, \overline{\mathbf{U}}_{j}) dx + \frac{1}{\Delta x_{j}^{n+1}} \int_{x_{j}^{n+1}}^{x_{j+\frac{1}{2}}^{n+1}} R(x/t, \overline{\mathbf{U}}_{j}, \overline{\mathbf{U}}_{j+1}) dx$$
(4.3)

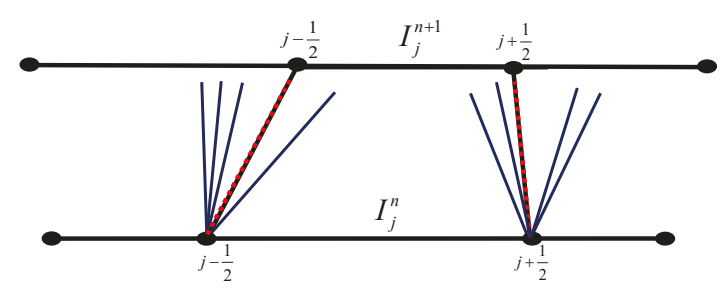


Figure 4.1: The HLLC Riemann solver performed along the Lagrangian cell's boundaries.

where $R(x/t, \overline{\mathbf{U}}_{j-1}, \overline{\mathbf{U}}_j)$ is the approximate Riemann solution between the states $\overline{\mathbf{U}}_{j-1}$ and $\overline{\mathbf{U}}_j$. The similar definition is for $R(x/t, \overline{\mathbf{U}}_j, \overline{\mathbf{U}}_{j+1})$. Specifically, for the HLLC Riemann solver, $R(x/t, \overline{\mathbf{U}}_{j-1}, \overline{\mathbf{U}}_j)$ in the relevant integration interval will take the value of either \mathbf{U}_R^* (calculated from the two states $\overline{\mathbf{U}}_{j-1}$ and $\overline{\mathbf{U}}_j$) or $\overline{\mathbf{U}}_j$. Similarly $R(x/t, \overline{\mathbf{U}}_j, \overline{\mathbf{U}}_{j+1})$ in the relevant integration interval will take the value of either $\overline{\mathbf{U}}_j$ or \mathbf{U}_L^* (calculated from the two states $\overline{\mathbf{U}}_j$ and $\overline{\mathbf{U}}_{j+1}$). Thus in order to prove the positivity-preserving property of the scheme (4.1), we only need to prove the intermediate states $\mathbf{U}_L^* \in G$, $\mathbf{U}_R^* \in G$ if $\mathbf{U}_L \in G$, $\mathbf{U}_R \in G$, which would imply that $\overline{\mathbf{U}}_j^{n+1}$ given by (4.3) also belongs to G, due to the fact that G is a convex set and Jensen's inequality for integrals. Next, we will prove if

$$\begin{cases}
\rho_L \ge 0, & e_{e,L} \ge 0, & e_{i,L} \ge 0, & e_{r,L} \ge 0 \\
\rho_R \ge 0, & e_{e,R} \ge 0, & e_{i,R} \ge 0, & e_{r,R} \ge 0
\end{cases} ,$$
(4.4)

then

$$\rho_L^* \ge 0, \qquad \qquad \rho_R^* \ge 0, \tag{4.5}$$

$$e_{e,L}^* \ge 0, \quad e_{i,L}^* \ge 0, \quad e_{r,L}^* \ge 0, \quad e_{e,R}^* \ge 0, \quad e_{i,R}^* \ge 0 \quad e_{r,R}^* \ge 0.$$
 (4.6)

under certain conditions.

Since $s_L \leq s_* \leq s_R$, from (3.15) it is easy to know (4.5) is valid. For simplicity, we only prove the validity of (4.6) for \mathbf{U}_L^* . Similar proof can be given for the validity for \mathbf{U}_R^* as well. To prove (4.6), for the γ -law gas, it is equivalent to prove

$$p_e^* \ge 0, \qquad p_i^* \ge 0, \qquad p_r^* \ge 0.$$
 (4.7)

From (3.16), we then need to prove

$$q_e \ge 0, \qquad q_i \ge 0, \qquad q_r \ge 0. \tag{4.8}$$

Take q_e as an example, from (3.15) and (3.17), we have,

$$q_e = \frac{A+B+C}{D},\tag{4.9}$$

where

$$A = \rho_L e_{e,L} (u_L - s_L)^2 + \rho_L \left(u_L \left(\frac{p_R - p_L}{3} + p_{e,L} \right) - u_R p_{e,R} \right) (u_L - s_L) - \frac{1}{12} (p_L - p_R)^2,$$

$$B = \rho_R e_{e,R} (s_R - u_R)^2 + \rho_R \left(u_R \left(\frac{p_R - p_L}{3} - p_{e,R} \right) + u_L p_{e,L} \right) (s_R - u_R) - \frac{1}{12} (p_L - p_R)^2,$$

$$C = (\rho_R e_{e,L} + \rho_R e_{e,R}) (u_L - s_L) (s_R - u_R) + \frac{1}{6} \rho_L \rho_R (u_L - s_L) (s_R - u_R) (u_L - u_R)^2,$$

$$D = \rho_L (u_L - s_L) + \rho_R (s_R - u_R).$$

$$(4.10)$$

Next we will prove A, B, C, D are positive under certain conditions.

If $s_L \leq u_L, s_R \geq u_R$, then we can prove $C, D \geq 0$. In order to make sure $A, B \geq 0, s_L, s_R$ should satisfy

$$s_{L} \leq u_{L} + \frac{\rho_{L}(u_{L}(\frac{p_{R}-p_{L}}{3} + p_{e,L}) - u_{R}p_{e,R})}{2\rho_{L}e_{e,L}}$$

$$-\frac{\sqrt{\rho_{L}^{2}(u_{L}(\frac{p_{R}-p_{L}}{3} + p_{e,L}) - u_{R}p_{e,R})^{2} + \frac{1}{3}\rho_{L}e_{e,L}(p_{L} - p_{R})^{2}}}{2\rho_{L}e_{e,L}} := s_{e,L},$$

$$s_{R} \geq u_{R} + \frac{\rho_{R}(u_{R}(\frac{p_{R}-p_{L}}{3} - p_{e,R}) + u_{L}p_{e,L})}{2\rho_{R}e_{e,R}}$$

$$+\frac{\sqrt{\rho_{R}^{2}(u_{R}(\frac{p_{R}-p_{L}}{3} - p_{e,R}) + u_{L}p_{e,L})^{2} + \frac{1}{3}\rho_{R}e_{e,R}(p_{L} - p_{R})^{2}}}{2\rho_{R}e_{e,R}} := s_{e,R}.$$

$$(4.11)$$

Similarly, we can obtain the following conditions for $q_i \geq 0, q_r \geq 0$,

$$s_{L} \leq u_{L} + \frac{\rho_{L}(u_{L}(\frac{p_{R}-p_{L}}{3} + p_{i,L}) - u_{R}p_{i,R})}{2\rho_{L}e_{i,L}}$$

$$-\frac{\sqrt{\rho_{L}^{2}(u_{L}(\frac{p_{R}-p_{L}}{3} + p_{i,L}) - u_{R}p_{i,R})^{2} + \frac{1}{3}\rho_{L}e_{i,L}(p_{L} - p_{R})^{2}}}{2\rho_{L}e_{i,L}} := s_{i,L},$$

$$s_{R} \geq u_{R} + \frac{\rho_{R}(u_{R}(\frac{p_{R}-p_{L}}{3} - p_{i,R}) + u_{L}p_{i,L})}{2\rho_{R}e_{i,R}}$$

$$+\frac{\sqrt{\rho_{R}^{2}(u_{R}(\frac{p_{R}-p_{L}}{3} - p_{i,R}) + u_{L}p_{i,L})^{2} + \frac{1}{3}\rho_{R}e_{i,R}(p_{L} - p_{R})^{2}}}{2\rho_{R}e_{i,R}} := s_{i,R}.$$

$$(4.12)$$

$$s_{L} \leq u_{L} + \frac{\rho_{L}(u_{L}(\frac{p_{R}-p_{L}}{3} + p_{r,L}) - u_{R}p_{r,R})}{2\rho_{L}e_{r,L}}$$

$$-\frac{\sqrt{\rho_{L}^{2}(u_{L}(\frac{p_{R}-p_{L}}{3} + p_{r,L}) - u_{R}p_{r,R})^{2} + \frac{1}{3}\rho_{L}e_{r,L}(p_{L} - p_{R})^{2}}}{2\rho_{L}e_{r,L}} := s_{r,L},$$

$$s_{R} \geq u_{R} + \frac{\rho_{R}(u_{R}(\frac{p_{R}-p_{L}}{3} - p_{r,R}) + u_{L}p_{r,L})}{2\rho_{R}e_{r,R}}$$

$$+\frac{\sqrt{\rho_R^2(u_R(\frac{p_R-p_L}{3}-p_{r,R})+u_Lp_{r,L})^2+\frac{1}{3}\rho_Re_{r,R}(p_L-p_R)^2}}{2\rho_Re_{r,R}}:=s_{r,R}.$$
 (4.13)

In summary, to preserve the positivity of the HLLC Riemann solver, s_L , s_R should satisfy

$$s_L = \min\{s_{e,L}, s_{i,L}, s_{r,L}\}, \qquad s_R = \max\{s_{e,R}, s_{i,R}, s_{r,R}\}.$$
 (4.14)

By the above discussion, we can obtain the following theorem for the Lagrangian scheme (4.1).

Theorem 4.1. Consider the first order finite volume Lagrangian scheme (4.1) with the HLLC flux (3.23) solving the 3-T equations (3.7) with the γ -law equation of state given by (2.3). If $\{\overline{U}_j \in G, \forall j = 1, ..., N\}$, then the scheme is positivity-preserving, that is, $\{\overline{U}_j^{n+1} \in G, \forall j = 1, ..., N\}$ if the HLLC numerical flux given by (3.23) is adopted with the acoustic wavespeeds s_L and s_R in (4.14) and with the time step restriction

$$\Delta t \le \lambda \min_{j=1,\dots,N} \frac{\Delta x_j}{|u_j| + (c_s)_j} \tag{4.15}$$

where the Courant number $\lambda = 0.5$.

4.2 The high order positivity-preserving Lagrangian scheme for the 3-T RH equations (3.7)-(3.8)

Assume the polynomial vector in the cell I_j obtained by the multi-resolution WENO reconstruction with degree k is $\mathbf{U}_j(x)$, where $k \geq 1$. $\mathbf{U}_{j+\frac{1}{2}}^- = \mathbf{U}_j(x_{j+\frac{1}{2}})$, $\mathbf{U}_{j-\frac{1}{2}}^+ = \mathbf{U}_j(x_{j-\frac{1}{2}})$ are applied in the numerical flux $\hat{\mathbf{F}}$. $\overline{\mathbf{U}}_j$ is the cell average of $\mathbf{U}_j(x)$ in I_j .

Consider a set of Gauss-Lobatto quadrature points in the cell I_j as

$$S_j = \{x_{j-\frac{1}{2}} = \tilde{x}_j^1, \tilde{x}_j^2, ..., \tilde{x}_j^{J-1}, \tilde{x}_j^J = x_{j+\frac{1}{2}}\}.$$

Define ω_{α} to be the quadrature weights such that $\omega_{\alpha} > 0, \alpha = 1, ..., J$ and $\sum_{\alpha=1}^{J} \omega_{\alpha} = 1$.

Next, we will show that if $\mathbf{U}_j(\tilde{x}_j^{\alpha}) \in G$ for all j and α , then $\overline{\mathbf{U}}_j^{n+1} \in G$ for the following high order Lagrangian scheme solving the 3-T RH equations (3.7)-(3.8) under suitable time step restriction,

$$\overline{\mathbf{U}}_{j}^{n+1} \Delta x_{j}^{n+1} - \overline{\mathbf{U}}_{j} \Delta x_{j} = -\Delta t \left(\hat{\mathbf{F}} (\mathbf{U}_{j+\frac{1}{2}}^{-}, \mathbf{U}_{j+\frac{1}{2}}^{+}) - \hat{\mathbf{F}} (\mathbf{U}_{j-\frac{1}{2}}^{-}, \mathbf{U}_{j-\frac{1}{2}}^{+}) \right). \tag{4.16}$$

We choose J to be the smallest integer satisfying $2J - 3 \ge k$, then the J-point Legendre Gauss-Lobatto rule is exact for the polynomial $\mathbf{U}_{i}(x)$, which means

$$\overline{\mathbf{U}}_{j} = \frac{1}{\Delta x_{j}} \int_{x_{j-\frac{1}{2}}}^{x_{j+\frac{1}{2}}} \mathbf{U}_{j}(x) dx = \sum_{\alpha=1}^{J} \omega_{\alpha} \mathbf{U}_{j}(\tilde{x}_{j}^{\alpha}) = \sum_{\alpha=2}^{J-1} \omega_{\alpha} \mathbf{U}_{j}^{\alpha} + \omega_{1} \mathbf{U}_{j-\frac{1}{2}}^{+} + \omega_{J} \mathbf{U}_{j+\frac{1}{2}}^{-}$$
(4.17)

where $\mathbf{U}_{j}^{\alpha} = \mathbf{U}_{j}(\tilde{x}_{j}^{\alpha})$. Here we take the three-point Simpson quadrature rule for the third order Lagrangian scheme (4.16), i.e. $S_{j} = \{x_{j-\frac{1}{2}}, x_{j}, x_{j+\frac{1}{2}}\}, \ \omega_{1} = \omega_{3} = \frac{1}{6}, \ \omega_{2} = \frac{2}{3}$.

By adding and subtracting $\Delta t \hat{\mathbf{F}}(\mathbf{U}_{j-\frac{1}{2}}^+, \mathbf{U}_{j+\frac{1}{2}}^-)$ in (4.16), it becomes

$$\overline{\mathbf{U}}_{j}^{n+1} \Delta x_{j}^{n+1} = \omega_{2} \mathbf{U}_{j}^{2} \Delta x_{j} + \omega_{1} \left(\mathbf{U}_{j-\frac{1}{2}}^{+} \Delta x_{j} - \frac{\Delta t}{\omega_{1}} (\hat{\mathbf{F}} (\mathbf{U}_{j-\frac{1}{2}}^{+}, \mathbf{U}_{j+\frac{1}{2}}^{-}) - \hat{\mathbf{F}} (\mathbf{U}_{j-\frac{1}{2}}^{-}, \mathbf{U}_{j-\frac{1}{2}}^{+}) \right)
+ \omega_{3} \left(\mathbf{U}_{j+\frac{1}{2}}^{-} \Delta x_{j} - \frac{\Delta t}{\omega_{3}} (\hat{\mathbf{F}} (\mathbf{U}_{j+\frac{1}{2}}^{-}, \mathbf{U}_{j+\frac{1}{2}}^{+}) - \hat{\mathbf{F}} (\mathbf{U}_{j-\frac{1}{2}}^{+}, \mathbf{U}_{j+\frac{1}{2}}^{-}) \right) \right)
= \omega_{2} \mathbf{U}_{j}^{2} \Delta x_{j} + \omega_{1} \hat{\mathfrak{F}}_{1} + \omega_{3} \hat{\mathfrak{F}}_{2}$$

where

$$\hat{\mathfrak{F}}_{1} = \mathbf{U}_{j-\frac{1}{2}}^{+} \Delta x_{j} - \frac{\Delta t}{\omega_{1}} (\hat{\mathbf{F}}(\mathbf{U}_{j-\frac{1}{2}}^{+}, \mathbf{U}_{j+\frac{1}{2}}^{-}) - \hat{\mathbf{F}}(\mathbf{U}_{j-\frac{1}{2}}^{-}, \mathbf{U}_{j-\frac{1}{2}}^{+})), \tag{4.18}$$

$$\hat{\mathfrak{F}}_{2} = \mathbf{U}_{j+\frac{1}{2}}^{-} \Delta x_{j} - \frac{\Delta t}{\omega_{3}} (\hat{\mathbf{F}}(\mathbf{U}_{j+\frac{1}{2}}^{-}, \mathbf{U}_{j+\frac{1}{2}}^{+}) - \hat{\mathbf{F}}(\mathbf{U}_{j-\frac{1}{2}}^{+}, \mathbf{U}_{j+\frac{1}{2}}^{-})). \tag{4.19}$$

We observe that the terms at the right hand side of both (4.18) and (4.19) have the same structure as that in the first order Lagrangian scheme (4.1), and $\omega_1 = \omega_3$. Thus if the HLLC numerical flux (3.23) with the acoustic wavespeeds (4.14) is adopted to determine $\hat{\mathbf{F}}$, then $\hat{\mathfrak{F}}_1$ and $\hat{\mathfrak{F}}_2$ are in the set G under the CFL condition

$$\Delta t \le \lambda \omega_1 \min_{j,\alpha} \frac{\Delta x_j}{|u_j^{\alpha}| + (c_s)_j^{\alpha}} \tag{4.20}$$

with $\lambda = 0.5$ and the sufficient condition

$$\mathbf{U}_{j}(\tilde{x}_{j}^{\alpha}) \in G, \ \forall \tilde{x}_{j}^{\alpha} \in S_{j}, \quad \alpha = 1, ..., J.$$
 (4.21)

Therefore we can summarize the above results in the following theorem.

Theorem 4.2. Consider the third order explicit Lagrangian scheme (4.16) solving the 3-T equations (3.7)-(3.8) with the γ -law equation of state given by (2.3). The HLLC numerical flux given by (3.23) is adopted where the acoustic wavespeeds are chosen as (4.14). If the reconstruction polynomial $U_j(x)$ for \overline{U}_j satisfies (4.21), then the scheme (4.16) is positivity-preserving, i.e., $\overline{U}_j^{n+1} \in G$ under the time step constraint (4.20) with $\lambda = 0.5$.

Under the assumption $\overline{\mathbf{U}}_j \in G$, in order to ensure the condition (4.21), we need to modify the multi-resolution WENO reconstruction polynomial $\mathbf{U}_j(x)$ used in the determination of $\hat{\mathbf{F}}$ into another polynomial

$$\widetilde{\mathbf{U}}_{i}(x) = \theta_{i}(\mathbf{U}_{i}(x) - \overline{\mathbf{U}}_{i}) + \overline{\mathbf{U}}_{i} \tag{4.22}$$

where $\theta_j \in [0, 1]$ is to be determined, such that $\widetilde{\mathbf{U}}_j(x) \in G, \forall x \in S_j$. Using the similar idea as in [29, 10, 11], we take the following specific steps for the implementation.

1. First, guarantee the positivity of density. Take a small number ϵ such as 10^{-13} so that $\overline{\rho}_j \geq \varepsilon$ for all j. In each cell I_j , compute

$$\widehat{\rho}_j(x) = \theta_j^0 \left(\rho_j(x) - \overline{\rho}_j \right) + \overline{\rho}_j, \quad \theta_j^0 = \min_{x \in S_j} \left\{ 1, \, \left| \frac{\overline{\rho}_j - \epsilon}{\overline{\rho}_j - \rho_j(x)} \right| \right\}. \tag{4.23}$$

2. Next, guarantee the positivity of the internal energy e_e, e_i, e_r for all the cells. Define $\widehat{\mathbf{U}}_j(x) = (\widehat{\rho}_j(x), (\rho u)_j(x), E_{e,j}(x), E_{i,j}(x), E_{r,j}(x))^T$. For each $x \in S_j$, set

$$\theta_x = \min\{\frac{e_e(\overline{\mathbf{U}}_j)}{e_e(\overline{\mathbf{U}}_j) - e_e(\widehat{\mathbf{U}}_j(x))}, \frac{e_i(\overline{\mathbf{U}}_j)}{e_i(\overline{\mathbf{U}}_j) - e_i(\widehat{\mathbf{U}}_j(x))}, \frac{e_r(\overline{\mathbf{U}}_j)}{e_r(\overline{\mathbf{U}}_j) - e_r(\widehat{\mathbf{U}}_j(x))}\}.$$

If $\theta_x > 1$ or $\theta_x < 0$, then set $\theta_x = 1$.

Finally we obtain the limited polynomial

$$\widetilde{\mathbf{U}}_{j}(x) = \theta_{j}^{1}(\widehat{\mathbf{U}}_{j}(x) - \overline{\mathbf{U}}_{j}) + \overline{\mathbf{U}}_{j}, \quad \theta_{j}^{1} = \min_{x \in S_{j}} \theta_{x}. \tag{4.24}$$

This positivity-preserving limiter can keep accuracy, conservation and positivity.

5 Two dimensional three temperature radiation hydrodynamics equations

In this section, we will briefly extend the above one-dimensional high order Lagrangian finite volume scheme to the two-dimensional case. We consider the two dimensional three-temperature radiation hydrodynamics equations,

$$\begin{cases}
\partial_{t}\rho + \partial_{x}\rho u + \partial_{y}\rho v = 0 \\
\partial_{t}\rho u + \partial_{x}\left(\rho u^{2} + p_{e} + p_{i} + p_{r}\right) + \partial_{y}\left(\rho u v\right) = 0 \\
\partial_{t}\rho v + \partial_{x}\left(\rho u v\right) + \partial_{y}\left(\rho v^{2} + p_{e} + p_{i} + p_{r}\right) = 0 \\
\partial_{t}\rho e_{e} + \partial_{x}\left(\rho e_{e} u\right) + \partial_{y}\left(\rho e_{e} v\right) + p_{e}(\partial_{x} u + \partial_{y} v) = \text{RHS}_{4} \\
\partial_{t}\rho e_{i} + \partial_{x}\left(\rho e_{i} u\right) + \partial_{y}\left(\rho e_{i} v\right) + p_{i}(\partial_{x} u + \partial_{y} v) = \text{RHS}_{5} \\
\partial_{t}\rho e_{r} + \partial_{x}\left(\rho e_{r} u\right) + \partial_{y}\left(\rho e_{r} v\right) + p_{r}(\partial_{x} u + \partial_{y} v) = \text{RHS}_{6}
\end{cases}$$
(5.1)

where

$$\begin{cases}
RHS_4 = \partial_x(\kappa_e\partial_x T_e) + \partial_y(\kappa_e\partial_y T_e) - \omega_{ei}(T_e - T_i) - \omega_{er}(T_e^4 - T_r^4) \\
RHS_5 = \partial_x(\kappa_i\partial_x T_i) + \partial_y(\kappa_i\partial_y T_i) + \omega_{ei}(T_e - T_i) \\
RHS_6 = \partial_x(\kappa_r\partial_x T_r^4) + \partial_y(\kappa_r\partial_y T_r^4) + \omega_{er}(T_e^4 - T_r^4)
\end{cases} (5.2)$$

and u, v are velocities in the x, y directions respectively, $\{e_e, e_i, e_r\}, \{\kappa_e, \kappa_i, \kappa_r\}, \{T_e, T_i, T_r\}$ are defined as before. We introduce the following new "energy" variables

$$E_e = \rho e_e + \frac{1}{6}\rho(u^2 + v^2), \ E_i = \rho e_i + \frac{1}{6}\rho(u^2 + v^2), \ E_r = \rho e_r + \frac{1}{6}\rho(u^2 + v^2),$$

and rewrite (5.1) as

$$\begin{cases} \partial_{t}\rho + \partial_{x}\rho u + \partial_{y}\rho v = 0 \\ \partial_{t}\rho u + \partial_{x}\left(\rho u^{2} + p_{e} + p_{i} + p_{r}\right) + \partial_{y}\left(\rho u v\right) = 0 \\ \partial_{t}\rho v + \partial_{x}\left(\rho u v\right) + \partial_{y}\left(\rho u v + p_{e} + p_{i} + p_{r}\right) = 0 \\ \partial_{t}E_{e} + \partial_{x}\left((E_{e} + p_{e})u\right) + \partial_{y}\left((E_{e} + p_{e})v\right) - \frac{u}{3}\partial_{x}\left(2p_{e} - p_{i} - p_{r}\right) - \frac{v}{3}\partial_{y}\left(2p_{e} - p_{i} - p_{r}\right) = \text{RHS}_{4} \\ \partial_{t}E_{i} + \partial_{x}\left((E_{i} + p_{i})u\right) + \partial_{y}\left((E_{i} + p_{i})v\right) - \frac{u}{3}\partial_{x}\left(2p_{i} - p_{r} - p_{e}\right) - \frac{v}{3}\partial_{y}\left(2p_{i} - p_{r} - p_{e}\right) = \text{RHS}_{5} \\ \partial_{t}E_{r} + \partial_{x}\left((E_{r} + p_{r})u\right) + \partial_{y}\left((E_{r} + p_{r})v\right) - \frac{u}{3}\partial_{x}\left(2p_{r} - p_{e} - p_{i}\right) - \frac{v}{3}\partial_{y}\left(2p_{r} - p_{e} - p_{i}\right) = \text{RHS}_{6} \end{cases}$$

$$(5.3)$$
Denote $\mathbf{U} = (\rho, \rho u, \rho v, E_{e}, E_{i}, E_{r})^{T}$, and we can represent the equations (5.3) in the reference

frame of a moving control volume in the integral form as

$$\frac{d}{dt} \int_{\Omega(t)} \mathbf{U} d\Omega + \int_{\Gamma(t)} \mathbf{F}(\mathbf{U}) d\Gamma + \int_{\Omega(t)} \mathbf{N}(\mathbf{U}) d\Omega = \int_{\Gamma(t)} \mathbf{G}(\mathbf{U}) d\Gamma + \int_{\Omega(t)} \mathbf{S}(\mathbf{U}) d\Omega$$
 (5.4)

where

$$\mathbf{F}(\mathbf{U}) = \begin{pmatrix} 0 \\ pn_x \\ pn_y \\ p_e w \\ p_i w \\ p_r w \end{pmatrix}, \ \mathbf{N}(\mathbf{U}) = \begin{pmatrix} 0 \\ 0 \\ 0 \\ -\frac{1}{3}\binom{u}{v} \cdot \nabla(2p_e - p_i - p_r) \\ -\frac{1}{3}\binom{u}{v} \cdot \nabla(2p_i - p_e - p_r) \\ -\frac{1}{3}\binom{u}{v} \cdot \nabla(2p_r - p_e - p_i) \end{pmatrix}, \ \mathbf{G}(\mathbf{U}) = \begin{pmatrix} 0 \\ 0 \\ 0 \\ \kappa_e \boldsymbol{n} \cdot \nabla(T_e) \\ \kappa_i \boldsymbol{n} \cdot \nabla(T_i) \\ \kappa_r \boldsymbol{n} \cdot \nabla(T_i) \end{pmatrix},$$

and $\mathbf{S}(\mathbf{U}) = (0, 0, 0, -\omega_{ei}(T_e - T_i) - \omega_{er}(T_e^4 - T_r^4), \omega_{ei}(T_e - T_i), \omega_{er}(T_e^4 - T_r^4))^T$. Here, we define $w := un_x + vn_y$, $p = p_e + p_i + p_r$ and $\boldsymbol{n} = (n_x, n_y)^T$ is the outward unit normal vector of the boundary.

5.1 2D high order conservative Lagrangian scheme for the 3-T RH equations

5.1.1High order spatial discretization

The two-dimensional spatial domain Ω is discretized into $N_x \times N_y$ quadrilateral cells $\{I_{j,k}\}_{j,k=1}^{N_x,N_y}$ where N_x and N_y are the number of cells in the x and y directions, respectively. Each cell $I_{j,k}$ has four nodes $P_{j-\frac{1}{2},k-\frac{1}{2}}, P_{j-\frac{1}{2},k+\frac{1}{2}}, P_{j+\frac{1}{2},k-\frac{1}{2}}, P_{j+\frac{1}{2},k+\frac{1}{2}}$ and the coordinate of $P_{j+\frac{1}{2},k+\frac{1}{2}}$ is $(x_{j+\frac{1}{2},k+\frac{1}{2}},y_{j+\frac{1}{2},k+\frac{1}{2}})$, for all $1 \leq j \leq N_x$, $1 \leq k \leq N_y$. The fluid velocity $(u_{j+\frac{1}{2},k+\frac{1}{2}},v_{j+\frac{1}{2},k+\frac{1}{2}})$ are defined at the nodes and the variables $\overline{\mathbf{U}}_{j,k} = (\overline{\rho}, \overline{M}^x, \overline{M}^y, \overline{E_e}, \overline{E_i}, \overline{E_r})_{j,k}^T$ solved directly are defined at the cell center $(x_{j,k},y_{j,k})$ in the form of cell averages,

$$\begin{split} \overline{\rho}_{j,k} &= \frac{1}{|I_{j,k}|} \int_{I_{j,k}} \rho dx dy, \ \overline{M}_{j,k}^x = \frac{1}{|I_{j,k}|} \int_{I_{j,k}} \rho u dx dy, \ \overline{M}_{j,k}^y = \frac{1}{|I_{j,k}|} \int_{I_{j,k}} \rho v dx dy, \\ (\overline{E_e})_{j,k} &= \frac{1}{|I_{j,k}|} \int_{I_{j,k}} E_e dx dy, \ (\overline{E_i})_{j,k} = \frac{1}{|I_{j,k}|} \int_{I_{j,k}} E_i dx dy, \ (\overline{E_r})_{j,k} = \frac{1}{|I_{j,k}|} \int_{I_{j,k}} E_r dx dy, \end{split}$$

where $M^x := \rho u$, $M^y := \rho v$ and $|I_{j,k}|$ is the area of the cell $I_{j,k}$. Then the semi-discrete finite volume scheme for the system follows as,

$$\frac{d}{dt}(\overline{\mathbf{U}}_{j,k}|I_{j,k}|) = -\int_{\partial I_{j,k}} \widehat{\mathbf{F}}(\mathbf{U}^{\text{in}}, \mathbf{U}^{\text{ex}}, \boldsymbol{n}) dl + \int_{\partial I_{j,k}} \widehat{\mathbf{G}}(\mathbf{U}, \boldsymbol{n}) dl
-\int_{I_{j,k}} \widetilde{\mathbf{N}}(\mathbf{U}, \mathbf{U}^{\text{in}}, \mathbf{U}^{\text{ex}}, \boldsymbol{n}) dx dy + \int_{I_{j,k}} \mathbf{S}(\mathbf{U}, \boldsymbol{n}) dx dy,$$
(5.5)

and these numerical fluxes $\hat{\mathbf{F}}$, $\hat{\mathbf{G}}$ are consistent with the physical fluxes in (5.4). \mathbf{U}^{in} and \mathbf{U}^{ex} are the values of the variables \mathbf{U} on the cell $I_{j,k}$ and its neighboring cell, respectively.

Suppose that the cell $I_{j,k}$ has M edges (for our case M=4) and the quadrature points on each edge are denoted as $(x_{\alpha}^m, y_{\alpha}^m)$ for $m=1, \dots, M$, $\alpha=1, \dots, K$, where we omit the subscript j, k. Then we can write the line integral for the numerical fluxes as

$$\int_{\partial I_{j,k}} \widehat{\mathbf{F}} dl \approx \sum_{m=1}^{M} |l^{m}| \sum_{\alpha=1}^{K} \omega_{\alpha} \widehat{\mathbf{F}} \left(\mathbf{U}^{\text{in}}(x_{\alpha}^{m}, y_{\alpha}^{m}), \mathbf{U}^{\text{ex}}(x_{\alpha}^{m}, y_{\alpha}^{m}), \boldsymbol{n}^{m} \right),
\int_{\partial I_{j,k}} \widehat{\mathbf{G}} dl \approx \sum_{m=1}^{M} |l^{m}| \sum_{\alpha=1}^{K} \omega_{\alpha} \widehat{\mathbf{G}} \left(\mathbf{U}^{m}(x_{\alpha}^{m}, y_{\alpha}^{m}), \boldsymbol{n}^{m} \right),$$
(5.6)

where ω_{α} , $\alpha = 1, \dots, K$ are the weights in the quadrature rule, $|l^m|$ represents the length of the edge l^m and $\mathbf{n}^m = (n_x^m, n_y^m)^T$ is the outward unit normal vector of l^m . In fact, we use the Gauss-Lobatto quadrature rule, where (x_1^m, y_1^m) and (x_K^m, y_K^m) are the two endpoints of the edge l^m , and in this work we take K = 3. The other two integral terms can be written as

$$\int_{I_{j,k}} \widetilde{\mathbf{N}} dx dy \approx |I_{j,k}| \overline{\mathbf{N}}_{j,k} + \sum_{m=1}^{M} |l^m| \sum_{\alpha=1}^{K} \omega_{\alpha} \beta_{\alpha}^m \left[\mathbf{N} (\mathbf{U}^{\text{ex}}(x_{\alpha}^m, y_{\alpha}^m)) - \mathbf{N} (\mathbf{U}^{\text{in}}(x_{\alpha}^m, y_{\alpha}^m)) \right],
\int_{I_{j,k}} \mathbf{S} dx dy \approx |I_{j,k}| \overline{\mathbf{S}}_{j,k},$$
(5.7)

where $\beta_{\alpha}^{m} = \max\{-\frac{w_{\alpha}^{m}}{3}, 0\}$ and $\overline{\mathbf{S}}_{j,k}$, $\overline{\mathbf{N}}_{j,k}$ are the cell averages. $\mathbf{U}^{\text{in}}(x_{\alpha}^{m}, y_{\alpha}^{m})$ and $\mathbf{U}^{\text{ex}}(x_{\alpha}^{m}, y_{\alpha}^{m})$ are the values of the variables on the cell $I_{j,k}$ and its neighboring cell along the edge l^{m} in the advection term, respectively. $\mathbf{U}^{m}(x_{\alpha}^{m}, y_{\alpha}^{m})$ are the values of the variables on the common edge l^{m} in the diffusion term. Later, we will discuss how to get these values.

For the advection terms $\hat{\mathbf{F}}$, $\hat{\mathbf{N}}$, we utilize the multi-resolution WENO reconstruction [30, 31] method to reconstruct high-order polynomials for the variables on each cell $I_{j,k}$,

$$\mathbf{U}_{j,k}(x,y) = (\rho(x,y), M^x(x,y), M^y(x,y), E_e(x,y), E_i(x,y), E_r(x,y))_{j,k}^T.$$

With these polynomials, we can calculate the values at each quadrature point $\mathbf{U}^{\text{in}}(x_{\alpha}^m, y_{\alpha}^m)$ and $\mathbf{U}^{\text{ex}}(x_{\alpha}^m, y_{\alpha}^m)$ in $\widehat{\mathbf{F}}$ and $\widetilde{\mathbf{N}}$. Since we have given the description of the WENO reconstruction in the one-dimensional case in Section 3.1.1 and Section 3.1.4. For the simplicity, we will omit the details here.

For the diffusion term, we still follow the WENO idea to reconstruct high order polynomials $\mathbf{U}_{j,k}^m(x,y)$, on each edge l^m of the cell $I_{j,k}$, and these stencils should include the cells at the both sides of l^m , for stability. These WENO reconstruction polynomials can guarantee high order accuracy in the smooth region and avoid numerical oscillation near large gradient or shock regions. Then, we will use the values of the variables and their derivatives $\mathbf{U}_{j,k}^m(x,y)$, $\partial_x \mathbf{U}_{j,k}^m(x,y)$ and $\partial_y \mathbf{U}_{j,k}^m(x,y)$ to calculate $\partial_x T_e$, $\partial_y T_e$, $\partial_x T_i$, $\partial_y T_i$, $\partial_x T_r^4$, $\partial_y T_r^4$, on the cell boundary l^m for

$$\widehat{\mathbf{G}}\left(\mathbf{U}^{m}(x_{\alpha}^{m}, y_{\alpha}^{m}), \boldsymbol{n}^{m}\right) = \begin{pmatrix} 0 \\ 0 \\ \kappa_{e}n_{x}^{m}\partial_{x}T_{e}(\mathbf{U}^{m}(x_{\alpha}^{m}, y_{\alpha}^{m})) + \kappa_{e}n_{y}^{m}\partial_{y}T_{e}(\mathbf{U}^{m}(x_{\alpha}^{m}, y_{\alpha}^{m})) \\ \kappa_{i}n_{x}^{m}\partial_{x}T_{i}(\mathbf{U}^{m}(x_{\alpha}^{m}, y_{\alpha}^{m})) + \kappa_{i}n_{y}^{m}\partial_{y}T_{i}(\mathbf{U}^{m}(x_{\alpha}^{m}, y_{\alpha}^{m})) \\ \kappa_{r}n_{x}^{m}\partial_{x}T_{r}^{4}(\mathbf{U}^{m}(x_{\alpha}^{m}, y_{\alpha}^{m})) + \kappa_{r}n_{y}^{m}\partial_{y}T_{r}^{4}(\mathbf{U}^{m}(x_{\alpha}^{m}, y_{\alpha}^{m})) \end{pmatrix}.$$
(5.8)

We denote the two-dimensional HLLC numerical flux for the three-temperature equation (5.3) as,

$$\widehat{\mathbf{F}} = (\hat{F}_d, \hat{F}_m n_x, \hat{F}_m n_y, \hat{F}_e, \hat{F}_i, \hat{F}_r)^T.$$

Actually, the two-dimensional HLLC numerical flux is as same as the one-dimensional case (3.23) by substituting the velocities u_L, u_R, u^* into the normal velocities w_L, w_R, w^* , so we have,

$$w^* = \frac{\rho_L w_L (w_L - s_L) + \rho_R w_R (s_R - w_R) + p_L - p_R}{\rho_L (w_L - s_L) + \rho_R (s_R - w_R)},$$

where $w_L = u_L n_x + v_L n_y$, $w_R = u_R n_x + v_R n_y$, $w^* = u^* n_x + v^* n_y$. Following the same notations in (3.23), the HLLC numerical fluxes for the two-dimensional 3-T RH equations are,

$$\begin{cases}
\hat{F}_{d} = 0, \\
\hat{F}_{m} = \rho_{L} (w_{L} - w^{*}) (w_{L} - s_{L}) + p_{L}, \\
\hat{F}_{e} = -\frac{p_{e}^{*}}{\gamma_{L} - 1} (s_{*} - s_{L}) + \left(E_{e,L} - \frac{1}{6}\rho_{L} (w^{*})^{2}\right) (w_{L} - s_{L}) + p_{e,L} w_{L}, \\
\hat{F}_{i} = -\frac{p_{i}^{*}}{\gamma_{L} - 1} (s_{*} - s_{L}) + \left(E_{i,L} - \frac{1}{6}\rho_{L} (w^{*})^{2}\right) (w_{L} - s_{L}) + p_{i,L} w_{L}, \\
\hat{F}_{r} = -3p_{r}^{*} (s_{*} - s_{L}) + \left(E_{r,L} - \frac{1}{6}\rho_{L} (w^{*})^{2}\right) (w_{L} - s_{L}) + p_{r,L} w_{L},
\end{cases} (5.9)$$

under the assumption that $\gamma_e = \gamma_i$, $\gamma_r = \frac{4}{3}$.

For the derivatives $\partial_x p_e$, $\partial_y p_e$, $\partial_x p_i$, $\partial_y p_i$, $\partial_x p_r$, $\partial_y p_r$ in the non-conservative term **N**, we will use the values and derivative values of $\mathbf{U}_{j,k}(x,y)$ to approximate them, just like the one-dimensional case in (3.26).

Finally, we will use the reconstruction polynomials $\mathbf{U}_{j,k}(x,y)$ to approximate the values of temperatures T_e, T_i, T_r^4 in the energy-exchange terms \mathbf{S} .

5.1.2 The high order Runge-Kutta time discretization

Based on the two-dimensional semi-discrete Lagrangian scheme (5.5), combined with the first-order explicit Euler forward time discretization method, we have the following first-order explicit scheme

$$\overline{\mathbf{U}}_{j,k}^{n+1}|I_{j,k}^{n+1}| - \overline{\mathbf{U}}_{j,k}^{n}|I_{j,k}^{n}| = \Delta t \int_{\partial I_{j,k}^{n}} \left[-\widehat{\mathbf{F}}(\mathbf{U}^{n,\text{in}}, \mathbf{U}^{n,\text{ex}}, \boldsymbol{n}) + \widehat{\mathbf{G}}(\mathbf{U}^{n}, \boldsymbol{n}) \right] dt
+ \Delta t \int_{I_{j,k}^{n}} \left[-\widetilde{\mathbf{N}}(\mathbf{U}^{n}, \mathbf{U}^{n,\text{in}}, \mathbf{U}^{n,\text{ex}}, \boldsymbol{n}) + \mathbf{S}(\mathbf{U}^{n}, \boldsymbol{n}) \right] dx dy$$

$$= \Delta t \mathbf{L}(\overline{\mathbf{U}}_{j,k}) \tag{5.10}$$

where we denote $L(\overline{\mathbf{U}}_{j,k})$ as the spatial operator. Then, combined with the third order strong stability-preserving Runge-Kutta (SSP-RK) time discretization method [23, 18], we have the following two-dimensional high order explicit Lagrangian formulation,

Stage 1,

$$x_{j+\frac{1}{2},k+\frac{1}{2}}^{(1)} = x_{j+\frac{1}{2},k+\frac{1}{2}}^{n} + \Delta t u_{j+\frac{1}{2},k+\frac{1}{2}}^{n},$$

$$y_{j+\frac{1}{2},k+\frac{1}{2}}^{(1)} = y_{j+\frac{1}{2},k+\frac{1}{2}}^{n} + \Delta t v_{j+\frac{1}{2},k+\frac{1}{2}}^{n},$$

$$\overline{\mathbf{U}}_{j,k}^{(1)} |I_{j,k}^{(1)}| = \overline{\mathbf{U}}_{j,k}^{n} |I_{j,k}^{n}| + \Delta t \mathbf{L}(\overline{\mathbf{U}}_{j,k}^{n});$$
(5.11)

Stage 2,

$$x_{j+\frac{1}{2},k+\frac{1}{2}}^{(2)} = x_{j+\frac{1}{2},k+\frac{1}{2}}^{(1)} + \frac{1}{4}\Delta t \left[-3u_{j+\frac{1}{2},k+\frac{1}{2}}^{n} + u_{j+\frac{1}{2},k+\frac{1}{2}}^{(1)} \right],$$

$$y_{j+\frac{1}{2},k+\frac{1}{2}}^{(2)} = y_{j+\frac{1}{2},k+\frac{1}{2}}^{(1)} + \frac{1}{4}\Delta t \left[-3v_{j+\frac{1}{2},k+\frac{1}{2}}^{n} + v_{j+\frac{1}{2},k+\frac{1}{2}}^{(1)} \right],$$

$$\overline{\mathbf{U}}_{j,k}^{(2)}|I_{j,k}^{(2)}| = \overline{\mathbf{U}}_{j,k}^{(1)}|I_{j,k}^{(1)}| + \frac{1}{4}\Delta t \left[-3\mathbf{L}(\overline{\mathbf{U}}_{j,k}^{n}) + \mathbf{L}(\overline{\mathbf{U}}_{j,k}^{(1)}) \right];$$
(5.12)

Stage 3,

$$x_{j+\frac{1}{2},k+\frac{1}{2}}^{n+1} = x_{j+\frac{1}{2},k+\frac{1}{2}}^{n} + \frac{1}{6}\Delta t \left[u_{j+\frac{1}{2},k+\frac{1}{2}}^{n} + u_{j+\frac{1}{2},k+\frac{1}{2}}^{(1)} + 4u_{j+\frac{1}{2},k+\frac{1}{2}}^{(2)} \right],$$

$$y_{j+\frac{1}{2},k+\frac{1}{2}}^{n+1} = y_{j+\frac{1}{2},k+\frac{1}{2}}^{n} + \frac{1}{6}\Delta t \left[v_{j+\frac{1}{2},k+\frac{1}{2}}^{n} + v_{j+\frac{1}{2},k+\frac{1}{2}}^{(1)} + 4v_{j+\frac{1}{2},k+\frac{1}{2}}^{(2)} \right],$$

$$\overline{\mathbf{U}}_{j,k}^{n+1} |I_{j,k}^{n+1}| = \overline{\mathbf{U}}_{j,k}^{n} |I_{j,k}^{n}| + \frac{1}{6}\Delta t \left[\mathbf{L}(\overline{\mathbf{U}}_{j,k}^{n}) + \mathbf{L}(\overline{\mathbf{U}}_{j,k}^{(1)}) + 4\mathbf{L}(\overline{\mathbf{U}}_{j,k}^{(2)}) \right]. \tag{5.13}$$

In the next section, we will verify this two-dimensional Lagrangian scheme is high order accurate and non-oscillatory.

6 Numerical results

In this section, we perform some numerical experiments on our third order explicit Lagrangian schemes solving the 3-T RH equations (2.6) which is equivalent to (2.1). Purely Lagrangian computation are used to do all the following tests. The radiation constant a is taken to be 1 unless otherwise stated. The reference solutions for the following discontinuous problems are obtained by grid-refinement converged numerical solutions by the same scheme and are referred to as the "converged solutions".

6.1 The accuracy test

First we develop a manufactured solution to the system (2.1) to test the accuracy of our schemes. We add a source term $\mathbf{s} = (s_1, s_2, s_3, s_4, s_5)^T$ to the right hand side of (2.1) such that a given vector $\mathbf{U}(x)$ is a solution of the system (2.1). To be specific, we will solve the following equations,

$$\begin{cases} \partial_{t}\rho + \partial_{x}\rho u = s_{1} \\ \partial_{t}\rho u + \partial_{x}(\rho u^{2} + p_{e} + p_{i} + p_{r}) = s_{2} \\ \partial_{t}E_{e} + \partial_{x}((E_{e} + p_{e})u) - \frac{1}{3}u\partial_{x}(2p_{e} - p_{i} - p_{r}) = \partial_{x}(\kappa_{e}\partial_{x}T_{e}) - \omega_{ei}(T_{e} - T_{i}) - \omega_{er}(T_{e}^{4} - T_{r}^{4}) + s_{3} \\ \partial_{t}E_{i} + \partial_{x}((E_{i} + p_{i})u) - \frac{1}{3}u\partial_{x}(2p_{i} - p_{e} - p_{r}) = \partial_{x}(\kappa_{i}\partial_{x}T_{i}) + \omega_{ei}(T_{e} - T_{i}) + s_{4} \\ \partial_{t}E_{r} + \partial_{x}((E_{r} + p_{r})u) - \frac{1}{3}u\partial_{x}(2p_{r} - p_{e} - p_{i}) = \partial_{x}(\kappa_{r}\partial_{x}T_{r}^{4}) + \omega_{er}(T_{e}^{4} - T_{r}^{4}) + s_{5}. \end{cases}$$

$$(6.1)$$

It has the following exact solutions,

$$\begin{cases}
\rho(x,t) = 1 + 0.5\sin(x+t) \\
u(x,t) = 2 + \cos(x+t) \\
\rho e_e(x,t) = b_1(1 + b_2\cos(x+t)) \\
\rho e_i(x,t) = b_1(1 + b_2\sin(x+t)) \\
\rho e_r(x,t) = b_3(1 + b_4\cos(x+t))
\end{cases} (6.2)$$

where $\gamma_e = \gamma_i = \frac{5}{3}$. $w_{ei} = w_{er} = 1$. $\kappa_e = \kappa_i = \kappa_r = 1$. In this test, the initial computational domain is $[0, 2\pi]$. The initial condition is obtained by (6.2) with t = 0. The periodic boundary condition is applied.

We test the problem with $b_1 = 3$, $b_2 = 0.2$, $b_3 = 2$, $b_4 = 0.1$. Tables 6.1 shows the errors and orders for the our third order Lagrangian scheme. In the table, we observe that the scheme achieves third order accuracy both in L_1 and L_{∞} norms for all the variables we solve.

6.2 The non-oscillatory tests

In some of the following tests, to minimize the effect of the boundary condition, we duplicate the wave symmetrically and extend it periodically so that we could apply the periodic boundary conditions at the boundaries.

Table 6.1: Errors and orders for the accuracy test performed by the one-dimensional third order Lagrangian scheme solving one-dimensional 3-T RH equations (2.6) at t = 1

N	L	ρ	k	ρu	k	E_e	k	E_i	k	E_r	k
40	L_1	7.37E-4		3.28E-3		3.78E-3		4.55E-3		6.47E-3	
	L_{∞}	3.65E-3		1.99E-2		2.08E-2		2.54E-2		1.91E-2	
80	L_1	4.83E-5	3.93	1.99E-4	4.05	2.09E-4	4.18	2.47E-4	4.20	3.96E-4	4.03
	L_{∞}	1.25E-4	4.87	2.04E-3	3.29	1.59E-3	3.70	1.54E-3	4.04	1.72E-3	3.48
160	L_1	6.56E-6	2.88	1.41E-5	3.82	1.65E-5	3.67	2.65E-5	3.22	3.56E-5	3.47
	L_{∞}	1.49E-5	3.07	1.04E-4	4.29	9.32E-5	4.09	5.75E-5	4.74	1.10E-4	3.97
320	L_1	8.04E-7	3.03	1.28E-6	3.46	1.90E-6	3.12	3.20E-6	3.05	4.03E-6	3.14
	L_{∞}	1.88E-6	2.99	3.23E-6	5.01	6.26E-6	3.90	6.88E-6	3.06	1.26E-5	3.13
640	L_1	1.02E-7	2.98	1.51E-7	3.09	2.37E-7	3.00	3.63E-7	3.14	4.50E-7	3.16
	L_{∞}	2.36E-7	3.00	4.19E-7	2.95	7.66E-7	3.03	7.39E-7	3.22	1.52E-6	3.05

Example 1 (The 3-T double Lax radiative shock tube problem).

We first consider a one-dimensional double Lax shock tube problem with the initial computational domain [-10, 30]. The initial condition is

$$\begin{cases}
\rho = 0.445, & u = 0.698, & p_e = p_i = p_r = 1.176, & -10 \le x \le 0 \\
\rho = 0.5, & u = 0, & p_e = p_i = p_r = 0.19, & 0 \le x \le 20 \\
\rho = 0.445, & u = 0.698, & p_e = p_i = p_r = 1.176, & 20 \le x \le 30
\end{cases}$$
(6.3)

 $\gamma_e = \gamma_i = \frac{5}{3}$. The periodic boundary condition is applied. The results of our third order Lagrangian scheme with 200 initially uniform cells compared with the converged solution at t=1 are shown in Figure 6.1-6.2. In Figure 6.1, we give the numerical results of ρ , u, T_e , T_i , T_r obtained by our third order Lagrangian scheme solving the 3-T RH equations (2.6) with $w_{ei} = w_{er} = 0$ and $\kappa_e = \kappa_i = \kappa_r = 0$, which demonstrate that the magnitude and the position of the shocks are consistent with the converged solution well, there is no oscillation near the shocks. In Figure 6.2, we present the numerical results of our third order Lagrangian scheme solving the fully 3-T RH equations (2.6) with $w_{ei} = w_{er} = 1$ and $\kappa_e = \kappa_i = \kappa_r = 1$, where we observe that the solution is more smooth due to the effects of diffusion. The electron, ion and radiation have different temperatures at the final time due to the effect of energy exchange.

Example 2 (The 3-T RH problem of double two-interacting blast waves).

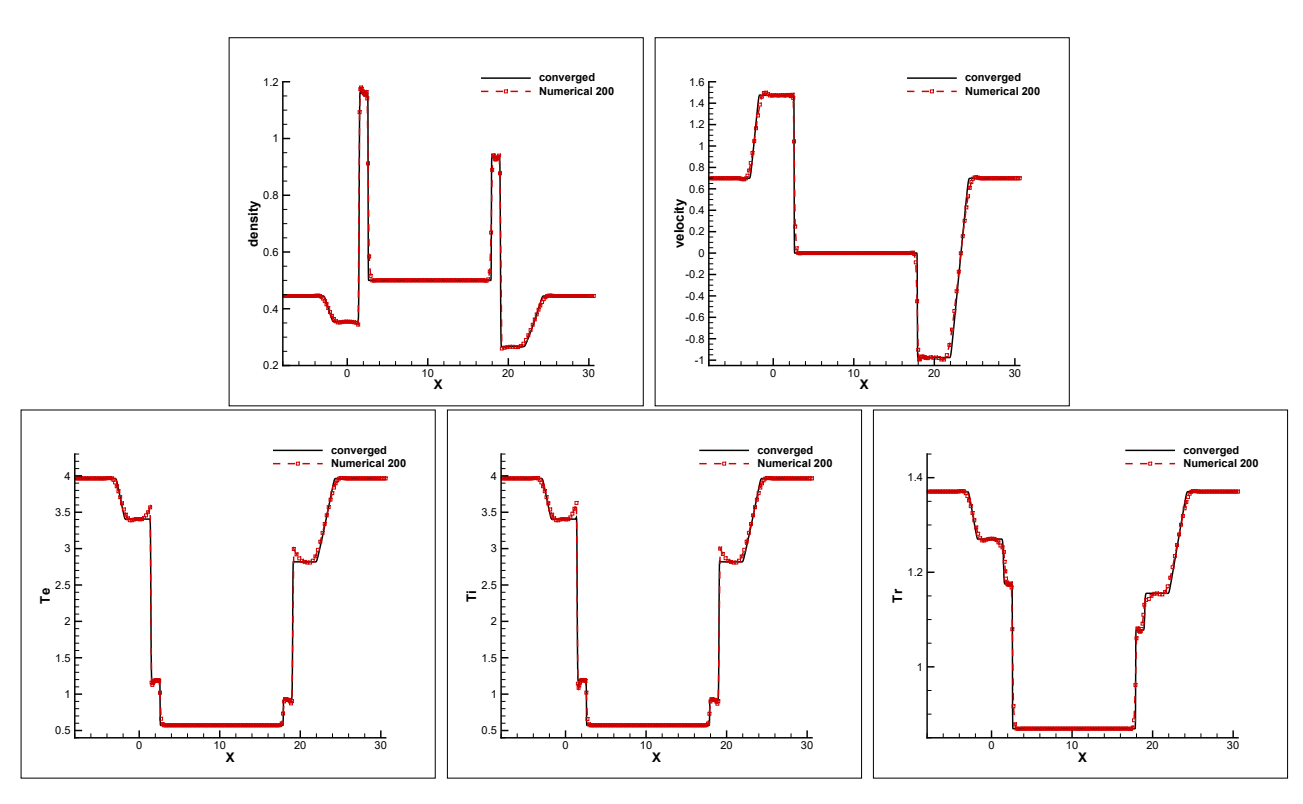


Figure 6.1: The numerical results of Example 1 with 200 cells against the converged solution at t=1 by using the third order Lagrangian scheme solving the 3-T RH equations (2.6) without the diffusion and energy-exchange terms. Left and Top: density, Right and Top: velocity, Left and Bottom: electron temperature, Middle and Bottom: ion temperature, Right and Bottom: radiation temperature.

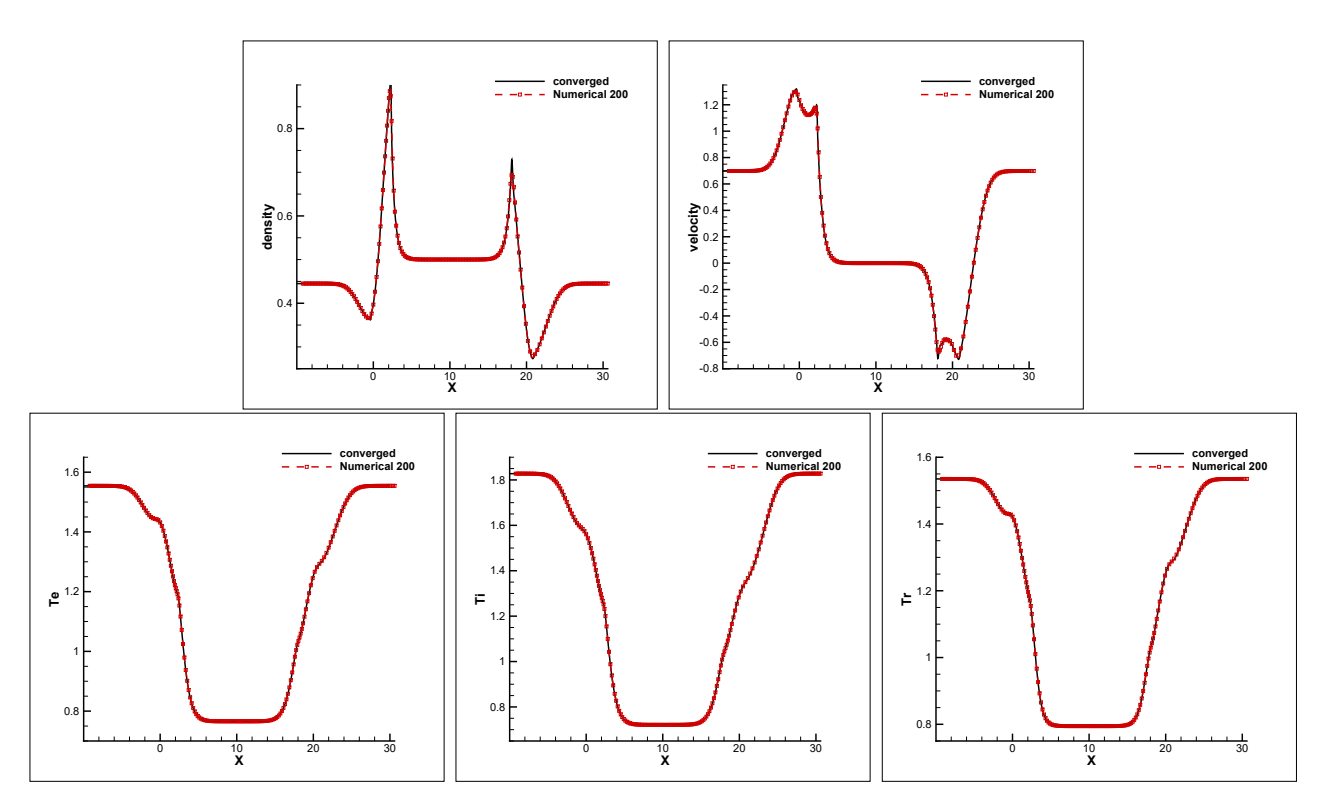


Figure 6.2: The results of Example 1 with 200 cells against the converged solution at t=1 by using the third order Lagrangian scheme solving the fully 3-T RH equations (2.6). Left and Top: density, Right and Top: velocity, Left and Bottom: electron temperature, Middle and Bottom: ion temperature, Right and Bottom: radiation temperature.

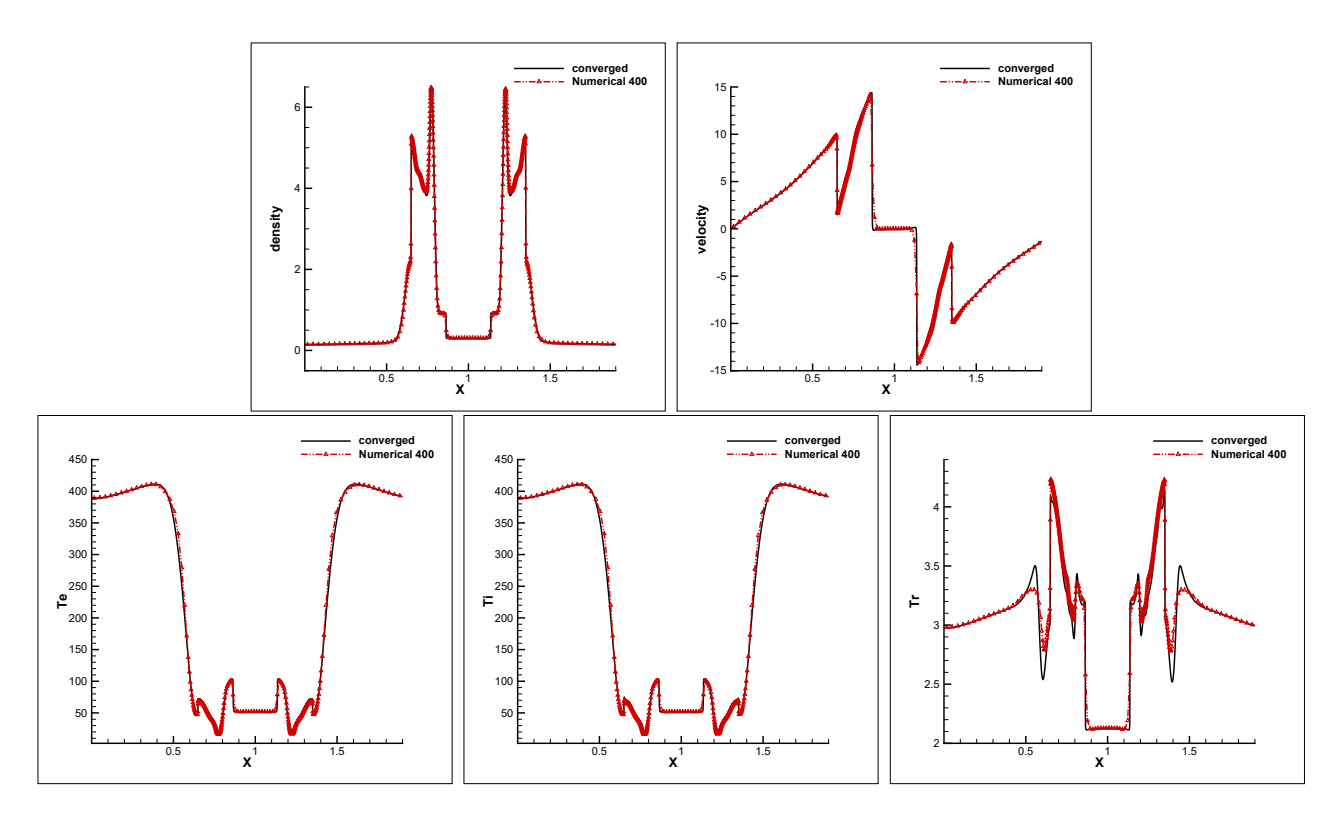


Figure 6.3: The results of Example 2 with 400 cells against the converged solution at t = 0.038 by using the third order Lagrangian scheme solving the 3-T RH equations (2.6). Left and Top: density, Right and Top: velocity, Left and Bottom: electron temperature, Middle and Bottom: ion temperature, Right and Bottom: radiation temperature.

For this problem, the initial condition is

$$\rho = 1, \quad u = 0, \quad p = \begin{cases}
1000, & 0 \le x \le 0.1 \\
0.01, & 0.1 \le x \le 0.9 \\
100, & 0.9 \le x \le 1.1 \\
0.01, & 1.1 \le x \le 1.9 \\
1000, & 1.9 \le x \le 2
\end{cases}, \quad p_e = p_i = p_r = \frac{1}{3}p. \quad (6.4)$$

The initial computational domain is [0, 2]. $\gamma_e = \gamma_i = 1.4$. $w_{ei} = w_{er} = 0$. $\kappa_e = \kappa_i = 0.01$, $\kappa_r = 0.001$. The periodic boundary condition is applied. The results of our third order explicit Lagrangian scheme solving the 3-T RH equations (2.6) with 400 initially uniform cells compared with the converged solution at t = 0.038 are shown in Figure 6.3. We can see the very satisfactory resolution and non-oscillation in the results of high order Lagrangian scheme.

Example 3 (The 3-T radiative shock tube problem involving two rarefaction waves).

This shock tube problem involves two rarefaction waves moving towards the opposite

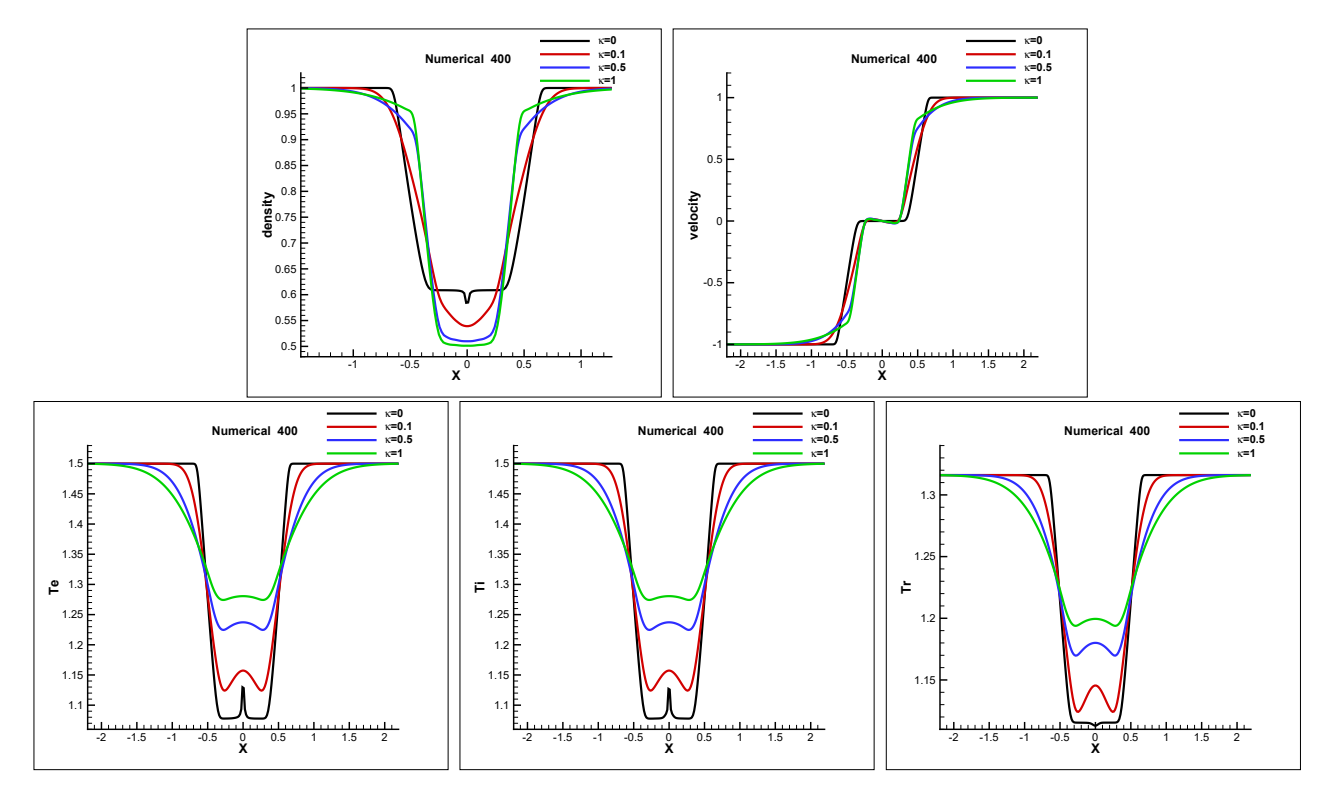


Figure 6.4: The results of Example 3 with the different κ_e , κ_i , κ_r at t = 0.2 by using the third order schemes solving the 3-T RH equations (2.6) with 400 cells. Left and Top: density, Right and Top: velocity, Left and Bottom: electron temperature, Middle and Bottom: ion temperature, Right and Bottom: radiation temperature.

directions. Its initial condition is

$$\begin{cases} \rho = 1, & u = -1, & p_e = p_i = p_r = 0.333333, & -2 \le x \le 0 \\ \rho = 1, & u = 1, & p_e = p_i = p_r = 0.333333, & 0 \le x \le 2 \end{cases}$$

$$(6.5)$$

 $\gamma_e = \gamma_i = \frac{5}{3}$. $w_{ei} = w_{er} = 0$. The Dirichlet boundary condition is applied at the boundaries. For this problem, we test the problem containing the diffusion terms with $\kappa_e = \kappa_i = \kappa_r = 0, 0.1, 0.5, 1$ respectively. Figure 6.4 shows the results of our third order Lagrangian scheme by using 400 cells at t = 0.2. We observe that the diffusion effect is more severe as $\kappa_e, \kappa_i, \kappa_r$ increases, which is quite reasonable with the common sense in physics.

Example 4 (The Shu-Osher 3-T RH problem).

For this problem, the initial condition is

$$\begin{cases} \rho = 3.857143, & u = 2.629369, & p_e = p_i = p_r = 3.444444, & -10 \le x \le -4 \\ \rho = 1 + \epsilon \sin kx, & u = 0, & p_e = p_i = p_r = 0.333333, & -4 \le x \le 15 \end{cases}$$
(6.6)

where ϵ and k are the amplitude and wave number of the entropy wave. In our test, we take $\epsilon = 0.2, k = 5$. $\gamma_e = \gamma_i = 1.4$. $w_{ei} = 1, w_{er} = 0.01$. $\kappa_e = \kappa_i = \kappa_r = 0.01$. The

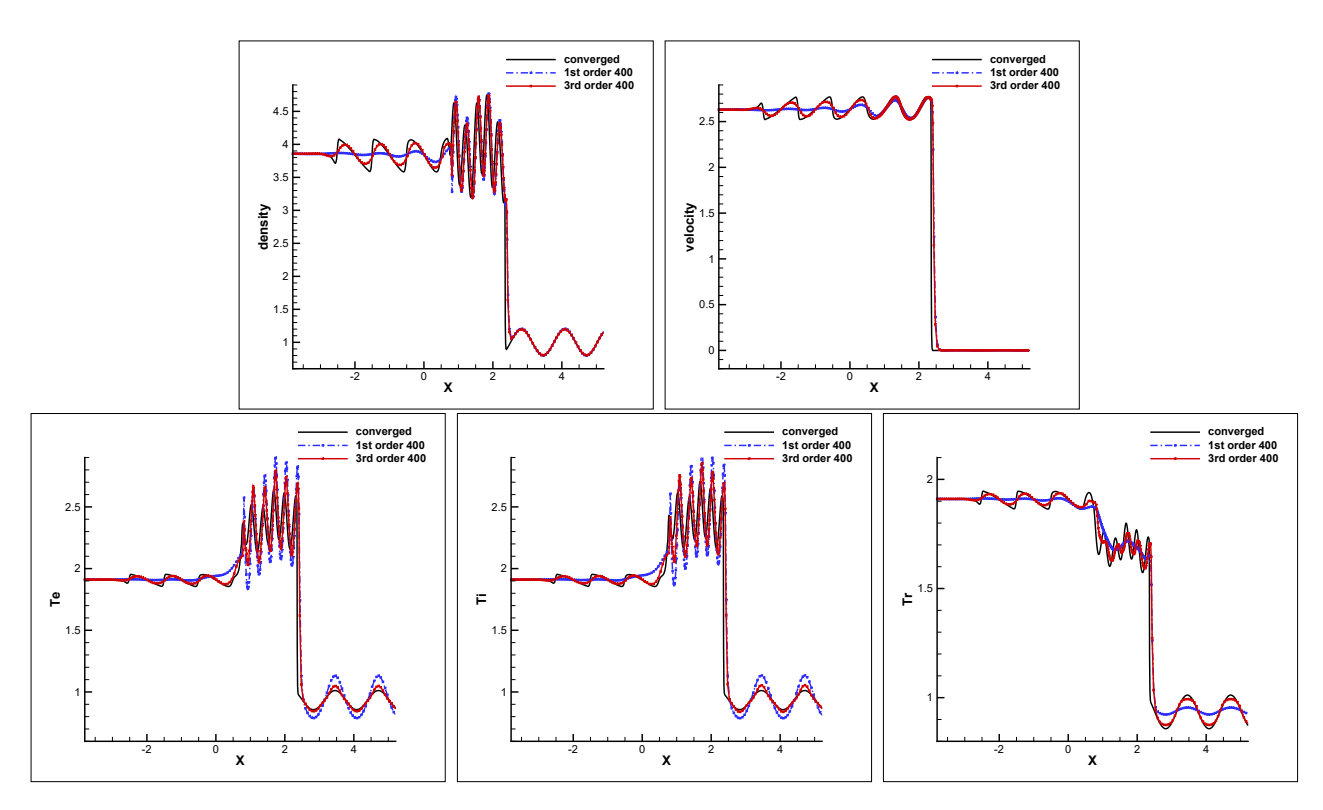


Figure 6.5: The results of Example 4 with 400 cells against the converged solution at t = 1.8 by using the first order and third order Lagrangian scheme solving the 3-T RH equations (2.6) respectively. Left and Top: density, Right and Top: velocity, Left and Bottom: electron temperature, Middle and Bottom: ion temperature, Right and Bottom: radiation temperature.

Dirichlet boundary condition is applied at the boundaries. The final time is t=1.8. This problem is very suitable for testing the advantage of a high order scheme when the solution contains both shocks and complex smooth structures. The comparison results of our first and third order explicit Lagrangian scheme solving (2.6) with 400 initially uniform cells compared with the converged solution at t=1.8 are shown in Figure 6.5. We observe that the third order scheme can capture the fine structure in the profiles of ρ , u, T_e , T_i , T_r much better than the first order scheme, which verifies the advantage of the high order scheme. Meanwhile, we observe some overshoots in the figures of ρ , T_e , T_i . Such overshoots are caused by the Lagrangian framework rather than by the high order WENO reconstruction, since this phenomenon appears and even is more severe in the first order Lagrangian scheme. This issue has been illustrated in our previous paper [7].

Example 5 (The steady-state 3-T radiative shock problem).

In [20], Johnson and Klein obtained a series of steady-state solutions for 3-T radiative shocks by using the relaxation-based approach. In the model they investigated, both electron

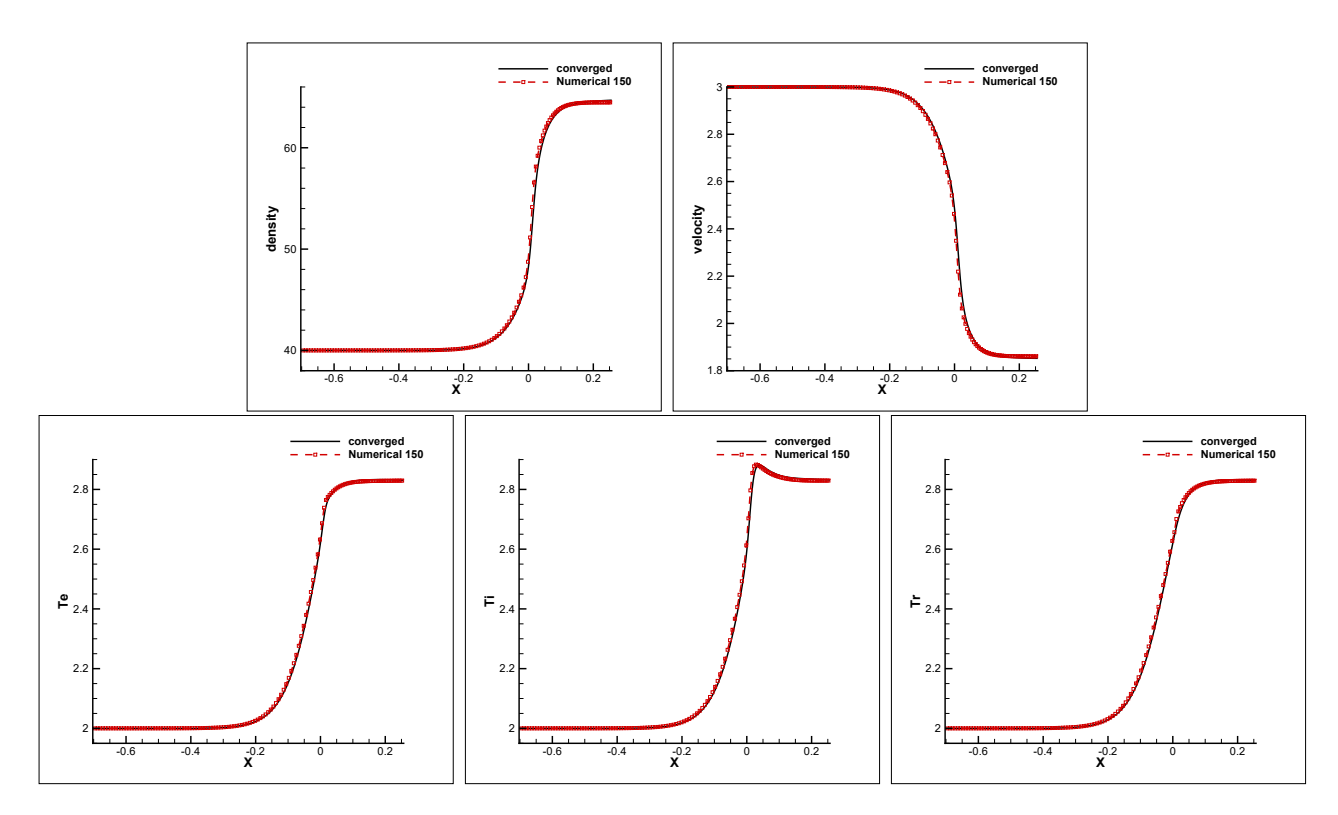


Figure 6.6: The results of Example 5 with 150 cells against the converged solution by using the third order Lagrangian scheme solving the 3-T RH equations (2.6). Left and Top: density, Right and Top: velocity, Left and Bottom: electron temperature, Middle and Bottom: ion temperature, Right and Bottom: radiation temperature.

and ion conduction are included, as well as ion viscosity. Here we test a similar 3-T radiative shock problem, in which the ion viscosity is not considered. The initial condition for the case with the Mach number M = 1.423025 is as follows,

$$\begin{cases}
\rho = 40, & u = 3, & T_e = T_i = T_r = 2, & -1 \le x \le 0 \\
\rho = 64.477616, & u = 1.861111, & T_e = T_i = T_r = 2.83044, & 0 \le x \le 0.5
\end{cases}$$
(6.7)

 $\gamma_e = \gamma_i = \frac{5}{3}$. $c_{ve} = c_{vi} = 1$. a = 0.01372. $w_{ei} = 6000$, $w_{er} = 411.320038$. $\kappa_e = 10^{-2}$, $\kappa_i = 10^{-5}$, $\kappa_r = 0.2$. The Dirichlet boundary condition is used at the boundaries. Figure 6.6 shows the steady state solution given by our third order Lagrangian scheme with 150 initially uniform cells. By comparison, we observe that our scheme can produce the non-oscillatory and high-resolution solution for this kind of 3-T radiation shock problems.

Example 6 (The multi-material 3-T radiative shock tube problem).

Last we consider a one-dimensional multi-material 3-T radiative shock tube problem.

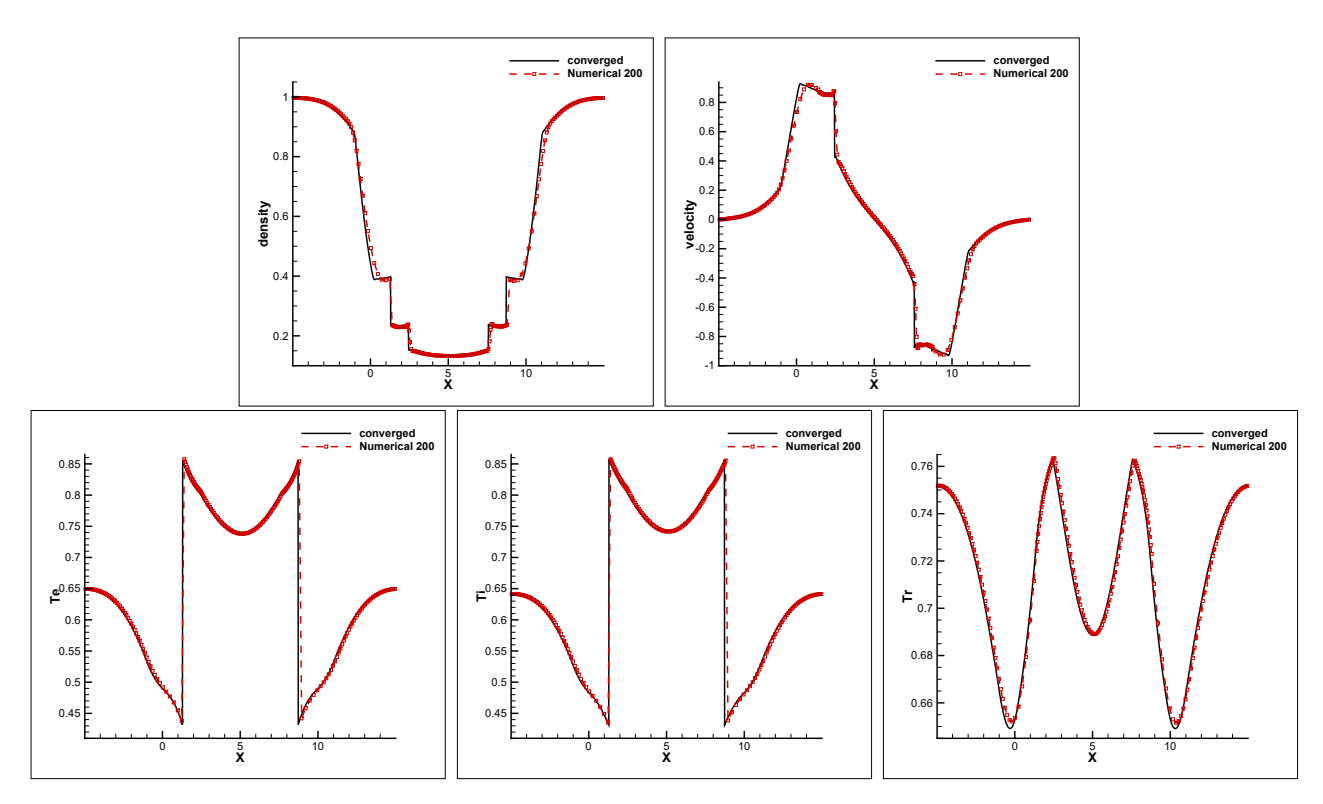


Figure 6.7: The results of Example 6 with 200 cells against the converged solution at t = 1.5 by using the third order Lagrangian scheme solving the 3-T RH equations (2.6). Left and Top: density, Right and Top: velocity, Left and Bottom: electron temperature, Middle and Bottom: ion temperature, Right and Bottom: radiation temperature.

The initial condition is

$$\begin{cases} \rho = 1, & u = 0, \\ \rho = 0.125, & u = 0, \end{cases} p_e = p_i = p_r = 0.3333333, \qquad \gamma_e = \gamma_i = \frac{7}{5}, \qquad -5 \le x \le 0 \\ \rho = 0.125, & u = 0, \qquad p_e = p_i = p_r = 0.0333333, \qquad \gamma_e = \gamma_i = \frac{5}{3}, \qquad 0 \le x \le 10 \\ \rho = 1, & u = 0, \qquad p_e = p_i = p_r = 0.3333333, \qquad \gamma_e = \gamma_i = \frac{7}{5}, \qquad 10 \le x \le 15 \end{cases}$$

$$(6.8)$$

The initial computational domain is [-5,15]. $w_{ei} = 10, w_{er} = 1$. $\kappa_e = \kappa_i = \kappa_r = 2$. The periodic boundary condition is applied. The results of our third order Lagrangian scheme with 200 initially uniform cells compared with the converged solution at t = 1.5 are shown in Figure 6.7. In the figures, we can see that the interface is very sharp and there is no oscillation near the interface, which verifies the advantage of the Lagrangian scheme and the capability of our scheme to treat multi-material problems.

6.3 The two-dimensional accuracy test

Next, we test the accuracy of our two-dimensional Lagrangian schemes for the system (5.1). In order to obtain the exact solution, an artificial source term is added to the right hand side of (5.1).

First, we take the velocities as constants u = v = 1, and the exact solutions follow as,

$$\begin{cases}
\rho(x,y,t) = 1 + 0.5\sin(x+y-2t) \\
u(x,y,t) = v(x,y,t) = 1 \\
\rho e_e(x,y,t) = b_1(1+b_2\sin(x+y-2t)) \\
\rho e_i(x,y,t) = b_1(1+b_2\cos(x+y-2t)) \\
\rho e_r(x,y,t) = b_3(1+b_4\sin(x+y-2t))
\end{cases}$$
(6.9)

where $\gamma_e = \gamma_i = \frac{5}{3}$. $w_{ei} = w_{er} = 0$. $\kappa_e = \kappa_i = \kappa_r = 0$. $b_1 = 3, b_2 = 0.2, b_3 = 2, b_4 = 0.1$. The initial computational domain is $[0, 2\pi] \times [0, 2\pi]$, and be uniformly divided into $N_x \times N_y$ rectangular cells. The periodic boundary condition is applied.

Table 6.2 shows the errors and orders for our two-dimensional third order Lagrangian scheme under different mesh sizes $N_x = N_y = 40, 80, 120, 160, 200$. In this table, we observe that the scheme achieves third order accuracy which verifies our spatial discretization and time discretization are both high order accurate. But taking u = v = 1 is too special which means that the meshes are only moving without any change in the cell shapes and sizes, hence higher order accuracy is observed.

Table 6.2: Errors and orders for the accuracy test performed by the two-dimensional high-order Lagrangian scheme solving the two-dimensional 3-T RH equations (5.1) at time t = 0.1 with the exact solutions (6.9).

N_x	L	ρ	k	ρu	k	E_e	k	E_i	k	E_r	k
40	L_1	2.59E-4		2.62E-4		5.02E-4		4.16E-4		2.34E-4	
	L_{∞}	8.02E-4		8.10E-4		1.34E-3		1.31E-3		6.80E-4	
80	L_1	3.23E-5	3.00	3.26E-5	3.01	6.34E-5	2.98	5.18E-5	3.01	3.05E-5	2.94
	L_{∞}	1.01E-4	2.99	1.02E-4	3.00	1.70E-4	2.98	1.69E-4	2.96	8.77E-5	2.95
120	L_1	9.56E-6	3.00	9.65E-6	3.00	1.92E-5	2.95	1.55E-5	2.98	9.49E-6	2.88
	L_{∞}	2.99E-5	3.00	3.01E-5	3.00	5.24E-5	2.91	5.16E-5	2.93	2.68E-5	2.93
160	L_1	4.03E-6	3.00	4.07E-6	3.00	8.32E-6	2.91	6.67E-6	2.93	4.20E-6	2.83
	L_{∞}	1.26E-5	3.00	1.27E-5	3.00	2.30E-5	2.87	2.24E-5	2.90	1.16E-5	2.90
200	L_1	2.06E-6	3.00	2.08E-6	3.00	4.39E-6	2.86	3.51E-6	2.87	2.26E-6	2.79
	L_{∞}	6.46E-6	3.00	6.49E-6	3.00	1.22E-5	2.84	1.18E-5	2.87	6.14E-6	2.87

Then, we take the velocities as the cosine function $u = v = 2 + \cos(x + y - 2t)$, and the exact solutions follow as.

$$\begin{cases}
\rho(x,y,t) = 1 + 0.5\sin(x+y-2t) \\
u(x,y,t) = v(x,y,t) = 2 + \cos(x+y-2t) \\
\rho e_e(x,y,t) = b_1(1+b_2\sin(x+y-2t)) \\
\rho e_i(x,y,t) = b_1(1+b_2\cos(x+y-2t)) \\
\rho e_r(x,y,t) = b_3(1+b_4\sin(x+y-2t))
\end{cases} (6.10)$$

where $\gamma_e = \gamma_i = \frac{5}{3}$. $w_{ei} = w_{er} = 0.1$. $\kappa_e = \kappa_i = \kappa_r = 0.5$. $b_1 = 3, b_2 = 0.2, b_3 = 2, b_4 = 0.1$. The initial computational domain and boundary condition are as same as the previous case.

Table 6.3 shows the errors and orders and we observe our two-dimensional Lagrangian scheme achieves second-order accuracy with the cosine velocities. This is expected as we are using a pure Lagrangian scheme with straight-line edged cells, hence the order of accuracy is restricted to two regardless of the orders of reconstruction and time discretization [8]. Curved cells or arbitrary Lagrangian-Eulerian (ALE) methods must be used to achieve higher than second order accuracy in 2D, which will be studied in the future.

Table 6.3: Errors and orders for the accuracy test performed by the two-dimensional high-order Lagrangian scheme solving the two-dimensional 3-T RH equations (5.1) at time t = 0.1 with the exact solutions (6.10).

N_x	L	ρ	k	ρu	k	E_e	k	E_i	k	E_r	k
40	L_1	1.39E-3		3.01E-3		6.92E-3		6.35E-3		4.79E-3	
	L_{∞}	2.99E-3		9.31E-3		1.78E-2		1.78E-2		1.50E-2	
80	L_1	3.35E-4	2.05	6.66E-4	2.18	1.64E-3	2.08	1.53E-3	2.05	1.10E-3	2.12
	L_{∞}	7.08E-4	2.08	1.84E-3	2.34	3.57E-3	2.32	3.51E-3	2.34	2.88E-3	2.38
120	L_1	1.47E-4	2.03	2.89E-4	2.06	7.14E-4	2.05	6.70E-4	2.04	4.77E-4	2.07
	L_{∞}	3.08E-4	2.06	7.61E-4	2.18	1.48E-3	2.17	1.43E-3	2.21	1.17E-3	2.22
160	L_1	8.23E-5	2.03	1.61E-4	2.04	3.97E-4	2.05	3.74E-4	2.03	2.63E-4	2.07
	L_{∞}	1.71E-4	2.04	4.11E-4	2.14	8.04E-4	2.12	8.38E-4	1.87	6.28E-4	2.16
200	L_1	5.24E-5	2.02	1.02E-4	2.05	2.51E-4	2.05	2.37E-4	2.04	1.65E-4	2.08
	L_{∞}	1.09E-4	2.03	2.56E-4	2.13	5.25E-4	1.91	5.54E-4	1.85	4.12E-4	1.89

6.4 The two-dimensional non-oscillatory test

We consider the two-dimensional 3-T double Lax radiative shock tube problem on a quarter of the circular domain $0 \le R \le 40$ with the initial condition as

$$\begin{cases}
\rho = 0.5, & u_R = 0, & p_e = p_i = p_r = 0.19, & 0 \le R \le 10, \\
\rho = 0.445, & u_R = 0.698, & p_e = p_i = p_r = 1.176, & 10 \le R \le 30, \\
\rho = 0.5, & u_R = 0, & p_e = p_i = p_r = 0.19, & 30 \le R \le 40,
\end{cases}$$
(6.11)

where $\gamma_e = \gamma_i = \frac{5}{3}$ and u_R is the radial velocity. The symmetric boundary condition is applied.

In Figure 6.8, we show the computational meshes with 200×10 cells and $w_{ei} = w_{er} = 0$, $\kappa_e = \kappa_i = \kappa_r = 0$ at time t = 0 and t = 1. We show the contours of density, electron temperature, ion temperature and radiation temperature in Figure 6.9 with $w_{ei} = w_{er} = 0$, $\kappa_e = \kappa_i = \kappa_r = 0$ and Figure 6.10 with $w_{ei} = w_{er} = 0.1$, $\kappa_e = \kappa_i = \kappa_r = 0.5$ on the 400×10 mesh respectively. The radial cuts of the results with 200×10 and 400×10 cells compared with the converged solution at t = 1 are shown in Figure 6.11 and Figure 6.12. From these results, we observe the positions of the contacts and shocks obtained by our two-dimensional high order Lagrangian scheme consist with the converged solution well, which

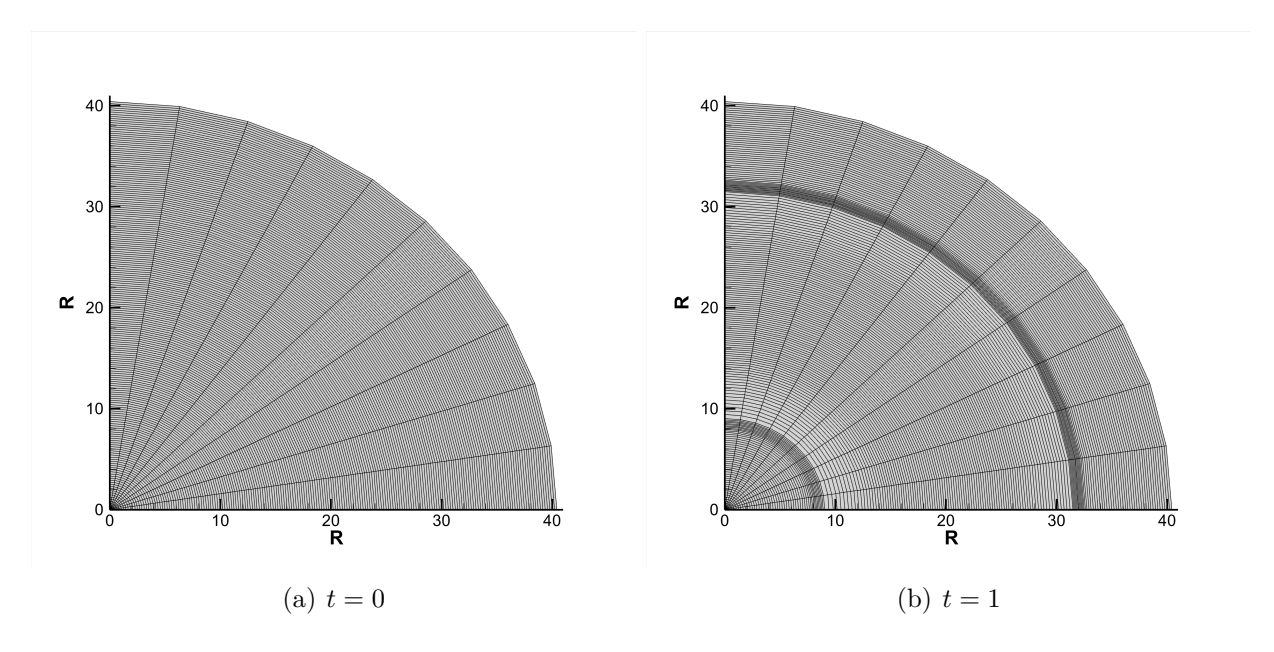


Figure 6.8: Computational meshes of the non-oscillation test at different time with 200×10 cells and $w_{ei} = w_{er} = 0$, $\kappa_e = \kappa_i = \kappa_r = 0$.

verifies the advantage of the Lagrangian scheme. Based on the WENO reconstruction, there is no oscillation near the contacts and shocks.

7 Concluding remarks

In this paper, we discuss the methodology to construct a class of high order conservative Lagrangian schemes for one and two dimensional three-temperature (3-T) radiation hydrodynamics (RH) equations. The 3-T RH equations contain the nonlinear advection, diffusion and relaxation terms which have different scales. Due to the nonconservative form of the

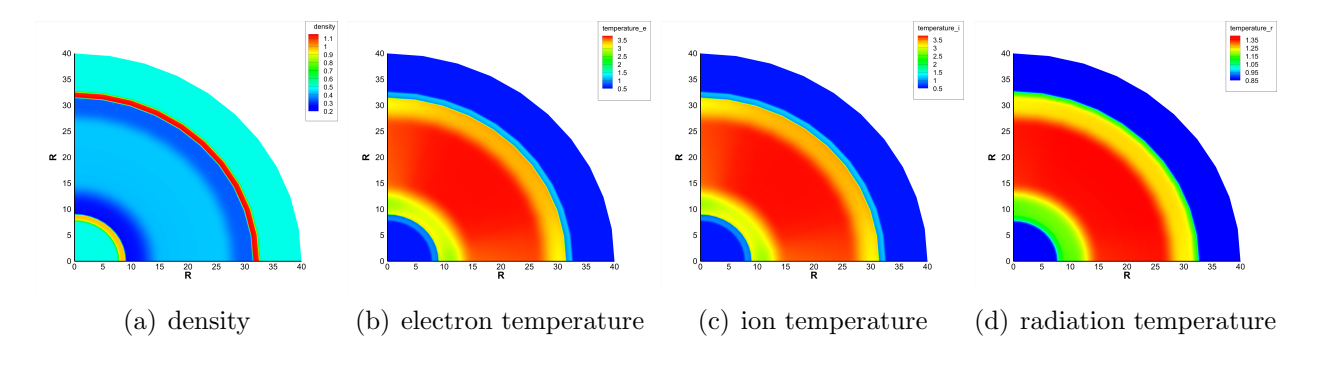


Figure 6.9: Contours of the two-dimensional non-oscillatory test with 400×10 cells at t = 1 by using the 2D high order Lagrangian scheme solving the 3-T RH equations (5.1) with $w_{ei} = w_{er} = 0$, $\kappa_e = \kappa_i = \kappa_r = 0$.

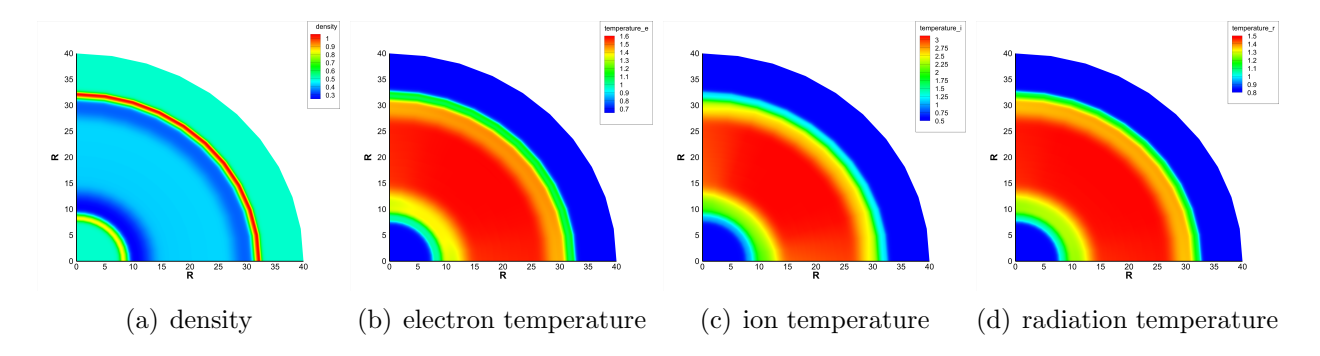


Figure 6.10: Contours of the two-dimensional non-oscillatory test with 400×10 cells at t=1 by using the 2D high order Lagrangian scheme solving the 3-T RH equations (5.1) with $w_{ei} = w_{er} = 0.1$, $\kappa_e = \kappa_i = \kappa_r = 0.2$.

3-T RH equations, it is difficult to design a high order and conservative scheme. In fact, there has been rare discussion on this topic in the literature so far. In order to design a Lagrangian scheme with both high order accuracy and the conservative property, we introduce three new energy variables, in the form of which the three energy equations of 3-T RH equations are rewritten. Based on the multi-resolution WENO reconstruction and the strong stability preserving (SSP) high order time discretizations, as an example, we design a class of conservative Lagrangian schemes with third order accuracy both in space and time. The methodology could be extended to arbitrary accuracy. We also develop an approximate HLLC Riemann solver for the Lagrangian scheme solving the 3-T RH equations which could be used to determine the numerical flux of the conservative advection terms in the equations. Furthermore, we prove the positivity-preserving property of a class of first order and high order Lagrangian schemes based on the above HLLC flux to solve the one-dimensional 3-T RH equations which only contain the conservative advection terms in space. The global positivity of the scheme is not guaranteed because the discretizations of the non-conservative terms, diffusion terms, and energy exchange terms have not been taken into consideration, which needs to be further investigated. Various numerical tests are given to verify the desired properties of the high order Lagrangian schemes such as high order accuracy, non-oscillation, conservation and adaptation to the multi-material problems. Preliminary extension to the two dimensional case is also considered. The design of the implicit high order conservative Lagrangian scheme, and more studies on the extension of the high order conservative Lagrangian schemes to multi-dimensional 3T RH equations, constitute our future work.

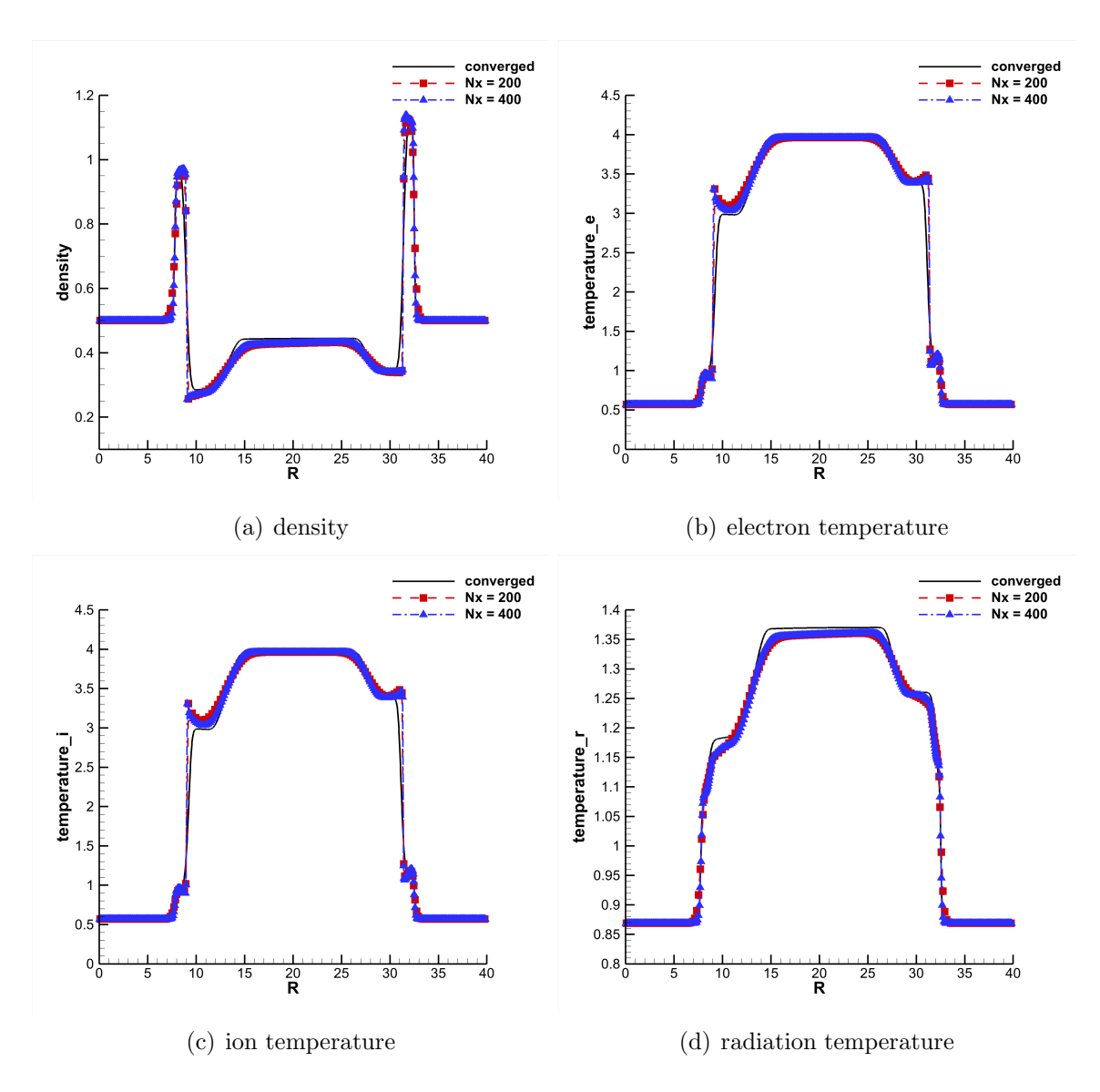


Figure 6.11: Radial cuts of the two-dimensional non-oscillatory test with 200×10 and 400×10 cells against the converged solution at t=1 by using the 2D high order Lagrangian scheme solving the 3-T RH equations (5.1) with $w_{ei}=w_{er}=0$, $\kappa_e=\kappa_i=\kappa_r=0$.

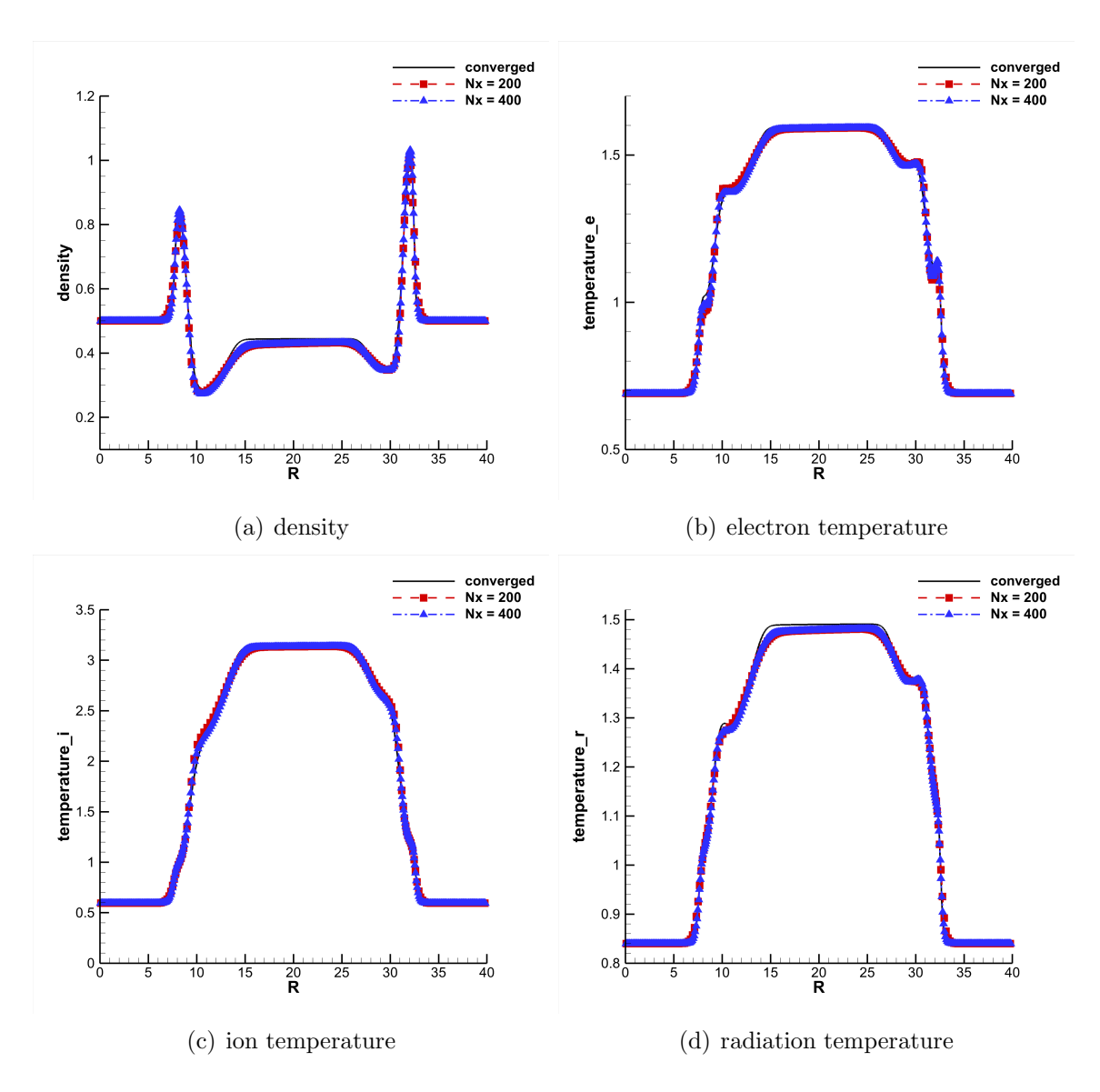


Figure 6.12: Radial cuts of the two-dimensional non-oscillatory test with 200×10 and 400×10 cells against the converged solution at t=1 by using the 2D high order Lagrangian scheme solving the 3-T RH equations (5.1) with $w_{ei}=w_{er}=0.1$, $\kappa_e=\kappa_i=\kappa_r=0.2$.

References

- [1] R. Abgrall and S. Karni, A comment on the computation of non-conservative products, Journal of Computational Physics, 229 (2010), 2759-2763.
- [2] R. Abgrall, P. Bacigaluppi and S. Tokareva, A high-order nonconservative approach for hyperbolic equations in fluid dynamics, Computers and Fluids, 169 (2018), 10-22.
- [3] S. Atzeni and J. Meyer-ter-Vehn *The Physics of Inertial Fusion: Beamplasma Interaction, Hydrodynamics, Hot Dense Matter*, Oxford University Press, 2004.
- [4] J. Breil, S. Galera and P.-H. Maire, Multi-material ALE computation in inertial confinement fusion code CHIC, Computers & Fluids, 46 (2011), 161-167.
- [5] M. Castro, B. Costa and W. S. Don, High order weighted essentially non-oscillatory WENO-Z schemes for hyperbolic conservation laws, Journal of Computational Physics, 230 (2011), 1766-1792.
- [6] R. Chauvin, S. Guisset and L. Martaud, A Colocalized Scheme for Three-Temperature Grey Diffusion Radiation Hydrodynamics, Communications in Computational Physics, 31 (2022), 293-330.
- [7] J. Cheng and C.-W. Shu, A high order ENO conservative Lagrangian type scheme for the compressible Euler equations, Journal of Computational Physics, 227 (2007), 1567-1596.
- [8] J. Cheng and C.-W. Shu, A third order conservative Lagrangian type scheme on curvilinear meshes for the compressible Euler equation, Communications in Computational Physics, 4 (2008), 1008-1024.
- [9] J. Cheng, C.-W. Shu and Q. Zeng. A conservative lagrangian scheme for solving compressible fluid flows with multiple internal energy equations, Communications in Computational Physics, 12 (2012), 1307-1328.
- [10] J. Cheng and C.-W. Shu, *Positivity-preserving Lagrangian scheme for multi-material compressible flow*, Journal of Computational Physics, 257 (2014), 143-168.
- [11] J. Cheng, C.-W. Shu and P. Song, High order conservative Lagrangian schemes for onedimensional radiation hydrodynamics equations in equilibrium limit, Journal of Computational Physics, 421 (2020), 109724.

- [12] Y. Cheng and C.-W. Shu, A discontinuous Galerkin finite element method for directly solving the Hamilton-Jacobi equations, Journal of Computational Physics, 223 (2007), 398-415.
- [13] R.P. Drake, Radiation Hydrodynamics, Springer-Verlag: Berlin Heidelberg, 2006.
- [14] C. Enaux, S. Guisset, C. Lasuen and Q. Ragueneau, Numerical resolution of a three temperature plasma model, Journal of Scientific Computing, 82 (2020), 51.
- [15] M. Fatenejad, B. Fryxell, J. Wohlbier, E. Myra, D. Lamb, C. Fryer and C. Graziani, Collaborative comparison of simulation codes for high-energy-density physics applications, High Energy Density Physics, 9 (2013), 63-66.
- [16] B. Fryxell, K. Olson, P. Ricker, F. X. Timmes, M. Zingale, D. Q. Lamb, P. Macneice, R. Rosner, J. W. Truran and H. Tufo, FLASH: An adaptive mesh hydrodynamics code for modeling astrophysical thermonuclear flashes, The Astrophysical Journal Supplement Series, 131 (2000), 273-334.
- [17] M. Gittings, R. Weaver, M. Clover, T. Betlach, N. Byrne, R. Coker, E. Dendy, R. Hueckstaedt, K. New, W. R. Oakes, D. Rantal and R. Stefan, *The RAGE radiation-hydrodynamic code*, Computational Science and Discovery, 1 (2008), 015005.
- [18] S. Gottlieb, C.-W. Shu and E. Tadmor, Strong stability-preserving high-order time discretization methods, SIAM Review, 43 (2001), 89-112.
- [19] B. van der Holst, G. Toth, I. V. Sokolov, K. G. Powell, J. P. Holloway, E. S. Myra, Q. Stout, M. L. Adams, J. E. Morel, S. Karni, B. Fryxell and R. P. Drake, CRASH: A block-adaptive-mesh code for radiative shock hydrodynamics implementation and verification, The Astrophysical Journal Supplement Series, 194 (2011), 23.
- [20] B. M. Johnson, R. I. Klein, Three-temperature plasma shock solutions with gray radiation diffusion, Shock Waves, 27 (2017), 281-289.
- [21] Y. Liu, C.-W. Shu and M. Zhang, Entropy stable high order discontinuous Galerkin methods for ideal compressible MHD on structured meshes, Journal of Computational Physics, 354 (2018), 163-178.
- [22] D. Mihalas and B. W. Mihalas, Foundations of Radiation Hydrodynamics, Oxford University Press, 1984.
- [23] C.-W. Shu and S. Osher, Efficient implementation of essentially non-oscillatory shock-capturing schemes, Journal of Computational Physics, 77 (1988), 439-471.

- [24] C.-W. Shu, T.A. Zang, G. Erlebacher, D. Whitaker and S. Osher, *High-order ENO schemes applied to two- and three-dimensional compressible flow*, Applied Numerical Mathematics, 9 (1992), 45-71.
- [25] T. Shiroto., S. Kawai and N. Ohnishi, Structure-preserving operators for thermal-nonequilibrium hydrodynamics, Journal of Computational Physics, 364 (2018), 1-17.
- [26] C.D. Sijoy and S. Chaturvedi, TRHD: Three-temperature radiation hydrodynamics code with an implicit non-equilibrium radiation transport using a cell-centered monotonic finite volume scheme on unstructured-grids, Computer Physics Communications, 190 (2015), 98-119.
- [27] C.D. Sijoy and S. Chaturvedi, Combining node-centered parallel radiation transport and higher-order multi-material cell-centered hydrodynamics methods in three-temperature radiation hydrodynamics code TRHD, Computer Physics Communications, 203 (2016), 94-109.
- [28] Q. Wargnier, S. Faure, B. Graille, T. Magin and M. Massot, Numerical treatment of the nonconservative product in a multiscale fluid model for plasmas in thermal nonequilibrium: application to solar physics, SIAM Journal on Scientific Computing, 42 (2020), b492-B519.
- [29] X. Zhang and C.-W. Shu, Positivity preserving high order discontinuous Galerkin schemes for compressible Euler equations with source terms, Journal of Computational Physics, 230 (2011), 1238-1248.
- [30] J. Zhu and C.-W. Shu, A new type of multi-resolution WENO schemes with increasingly higher order of accuracy, Journal of Computational Physics, 375 (2018), 659-683.
- [31] J. Zhu, C.-W. Shu, A new type of multi-resolution WENO schemes with increasingly higher order of accuracy on triangular meshes, Journal of Computational Physics, 392 (2019), 19-33.